nature portfolio

Peer Review File

Multi-stimulated far-UVC luminescence for solar-blind imaging

Corresponding Author: Professor Leipeng Li

This file contains all reviewer reports in order by version, followed by all author rebuttals in order by version.

Version 0:

Reviewer comments:

Reviewer #1

(Remarks to the Author)
This article presents a novel exploration of mechanoluminescence (ML) in lanthanide-doped SrF2, spanning a broad spectral range from ultraviolet to near-infrared. The corresponding advanced applications, including information encryption and high-level anti-counterfeiting, background-free marking, and structural monitoring, effectively pave the way for the development of secure and efficient systems. However, several issues should be addressed to enhance the clarity of the experimental procedures, strengthen the theoretical discussions, and improve the consistency of the presented data. Therefore, I recommend this manuscript should consider the following major revisions before the publication:
1.The present title is a little specific and needs to be revised appropriately.
2.How did the authors confirm the doping concentration (x%) in the synthesized SrF_2:x%Pr^{3+} (x = 0.1, 0.2, 0.5, 0.7, and 1) phosphors? If the doping concentrations were confirmed using techniques such as elemental mapping images or XPS profiles, the authors should clearly explain it in the Methods section. Additionally, if other techniques were employed to verify the doping levels, these should be clearly stated and described.
3.They mention that the materials prepared in this work exhibits the widest spectral range reported so far. A more comprehensive comparison with the existing ML materials is necessary to highlight the advancements made.
4.The paper discusses the trap-controlled ML mechanism but lacks detailed experimental verification. To strengthen the proposed mechanism, the authors should incorporate time-resolved luminescence or other dynamic studies to provide further evidence.
5.Although the role of X-ray pre-charging in enhancing ML is mentioned, the underlying processes remain insufficiently explored. It would be helpful for the authors to elaborate on how X-ray exposure specifically influences the charge trap states within the material and how these trapped charge carriers contribute to the enhanced ML. To further clarify the mechanism, the authors may consider adding theoretical calculations of relevant energy bands and defect states to provide a more comprehensive understanding of the processes involved.
6.The authors should provide additional ML data to further substantiate the self-recovering ML features of SrF_2: Pr^{3+}. And they should also add a comparison of the ML intensity before and after each cycle multiple cycles.
7.Please confirm the accuracy of the description in line 194: "… leaving there many holes in the conduction band." Additionally, when using the abbreviation "PMDC" for the first time, the authors should provide the full form to ensure that readers unfamiliar with the abbreviation can easily understand it.

Reviewer #2

(Remarks to the Author)
This manuscript reports the mechanoluminescence of Ln-doped SrF2, which is quite similar with the same authors' recent publications for ML in NaYF4:Pr3+ and Sr2P2O7:Pr3+. Besides the difference in host adopted, the authors try to highlight two innovations, i.e., the widest ML wavelength span (200nm to 1700nm) and the shortest ML wavelength (222nm). In my opinion, however, these two points are far from enough to persuade ones to support the publication of the present work in Nature Communications, due to the following issues.

1.UVC MLs are observed for all three Pr3+ doped phosphors (Sr2P2O7/NaYF4/SrF2). However, only the ML for SrF2:Pr3+ exhibits the transition of 4f5d→3H4 (222 nm). What is the origin for this difference? This question is crucial If the authors take "the shortest ML wavelength" so important. Unfortunately, the authors fails to give any explanation about it.

2.The wide ML wavelength span can be obtained by means of a serials of Ln2+,3+ doping/co-doping, which is quite easy to conceive by anyone. I don't think this point is a remarkable achievement.
3.Why there is no UVC components for PerL (Fig.3b)?
4.The authors spend a lot of efforts for the demonstration of the potential applications of ML of SrF2:Ln2+,3+ for information encryption and high-level anti-counterfeiting, background-free marking, and structural monitoring. The similar demonstrations for potential applications of ML materials have been well documented in many previous publications. For me, the present demonstrations do not bring any new information.

Reviewer #3

(Remarks to the Author)
In this paper, the authors developed a series of SrF2 crystals doped with various ions, including Ce3+, Pr3+, Nd3+, Sm3+, Eu2+/3+, Gd3+, Tb3+, Dy3+, Ho3+, Er3+, Tm3+, and Yb3+, effectively covering nearly all lanthanides known to serve as luminescent centers. These dopants enable the reported materials to exhibit mechanoluminescence (ML) across the broad wavelength range of 200–1700 nm. As noted by the reviewer, this is, to the best of our knowledge, the widest wavelength span reported within a single ML system. Furthermore, the Pr3+ ions in the SrF2 host produce ML in the 200–400 nm range, with a peak at ~222 nm, representing the shortest ML wavelength reported to date.

The development of new ML materials and the extension of the ML wavelength range are critical challenges for the ML research community. This paper makes a significant contribution to both areas. Additionally, the authors demonstrated potential applications of these materials, such as information encryption, high-level anti-counterfeiting, background-free marking, and structural monitoring. Based on these findings, the paper is recommended for publication, subject to addressing the following points:

Major Comments
1. Introduction: While the authors focus on the ML of lanthanides, previous studies have shown that some transition metal ions, such as Cr3+, also exhibit ML in appropriate hosts, with emission wavelengths extending to the near-infrared region. These references should be cited and discussed for completeness.
2. Role of Friction: The SrF2:0.5%Pr3+ sample shows weak ML before X-ray exposure. The authors attribute this to local piezoelectric properties induced by Pr3+, as evidenced by piezoresponse force microscopy (PFM). However, friction effects, which are frequently reported in ML studies, might also contribute. Additional experiments are necessary to confirm the role of friction in this phenomenon.
3. UV to Visible Emission Ratio: A comparison of the persistent luminescence (PersL) and ML spectra of SrF2:0.5%Pr3+ reveals a change in the intensity ratio of the UV to visible bands. The authors should provide a detailed discussion of this observation, as it may yield insights into the mechanisms underlying the various emission modes.
4. PersL and ML Correlation: The authors state that the PersL intensity is positively correlated with the ML of SrF2:Ln2+/3+ (Fig. 4b). A more thorough explanation of this correlation would enhance the understanding of the relationship between these two emission phenomena.

Minor Remarks
5. Figure 1: The overall tone of Figure 1 appears dim and is not visually striking. Consider enhancing the contrast or brightness to improve its appeal.
6. Figure 3a: There should be a space between the physical quantity "h" and the number "36."
7. Figure 4e: The labels for the horizontal and vertical axes appear to be reversed. Please correct this.

Version 1:

Reviewer comments:

Reviewer #1

(Remarks to the Author)
I consider that the authors have properly addressed the comments made by referees. The paper can be accepted for publication in the present form.

Reviewer #2

(Remarks to the Author)
The authors have addressed all my concerns and the manuscript can be accepted for publication.

Reviewer #3

(Remarks to the Author)
The authors have satisfactorily addressed all of my previous concerns, and the quality of the manuscript has been significantly improved in the revision. The broad spectral range (200–1700 nm) offers strong potential for diverse applications. I believe the manuscript is now suitable for publication in Nature Communications.

Point-by-point Responses (in blue) to the Reviewers' Comments (in black)

Reviewer #1:

This article presents a novel exploration of mechanoluminescence (ML) in lanthanide-doped SrF_2, spanning a broad spectral range from ultraviolet to near-infrared. The corresponding advanced applications, including information encryption and high-level anti-counterfeiting, background-free marking, and structural monitoring, effectively pave the way for the development of secure and efficient systems. However, several issues should be addressed to enhance the clarity of the experimental procedures, strengthen the theoretical discussions, and improve the consistency of the presented data. Therefore, I recommend this manuscript should consider the following major revisions before the publication:

Response:

Thank you for your high recognition of our article; this will encourage us to continue to deeply engage in research and development in novel and functional optical materials in the future. According to your invaluable comments and suggestions, we have carefully revised our manuscript. All changes are highlighted in blue in the revised manuscript, as detailed in the following point-to-point responses.

Comment 1: The present title is a little specific and needs to be revised appropriately.

Response:

We greatly appreciate the comment. As suggested, we have changed the title to 'Multi-stimulated far-UVC luminescence for solar-blind imaging'. Please see the new title in the revised manuscript.

Comment 2: How did the authors confirm the doping concentration (x%) in the synthesized SrF_2:x%Pr^{3+} (x = 0.1, 0.2, 0.5, 0.7, and 1) phosphors? If the doping concentrations were confirmed using techniques such as elemental mapping images or XPS profiles, the authors should clearly explain it in the Methods section. Additionally, if other techniques were employed to verify the doping levels, these should be clearly stated and described.

Response:

We greatly appreciate the comments. We used energy dispersive spectroscopy (EDS) to confirm the doping concentration (x%) in the synthesized SrF_2:x%Pr^{3+} (x = 0.1, 0.2, 0.5, 0.7 and 1) phosphors. The following figures (Supplementary Figs. 3–7) show the measured results, including the elemental distribution mappings and element ratios. Clearly, the results matched well with the expectations.

In the 'Material synthesis and characterization' part of 'Results' section, we have added the following sentences, 'The energy dispersive spectroscopy (EDS) results proved that the element ratios of Sr, F and Pr were as expected (Supplementary Figs. 3–7).'. Please see these changes on page 6 in the revised manuscript.

In the 'Material characterization' part of 'Methods' section, we have added the following sentences, 'The morphological and elemental composition analyses of samples were performed using an SEM instrument (FEI Nova Nano SEM450) equipped with an EDS detector.'. Please see these changes on page 15 in the revised manuscript.

Moreover, the following figures have been added to the Supplementary Information file (Supplementary Figs. 3–7).

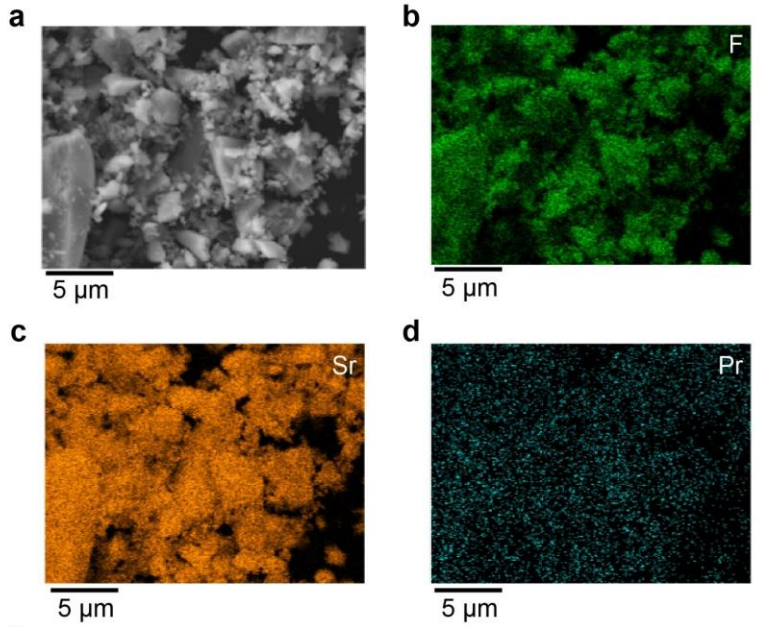

f

Element	Signal type	Weight %	Atomic %	Error % (Weight %)
F	EDS	29.79	66.19	0.12
Sr	EDS	70.10	33.77	0.14
Pr	EDS	0.11	0.03	0.12

Supplementary Fig. 3. (a) SEM image, (b) F, (c) Sr, and (d) Pr elemental mappings, (e) EDS spectrum and (f) Elemental analysis data of SrF_2:0.1%Pr^{3+}.

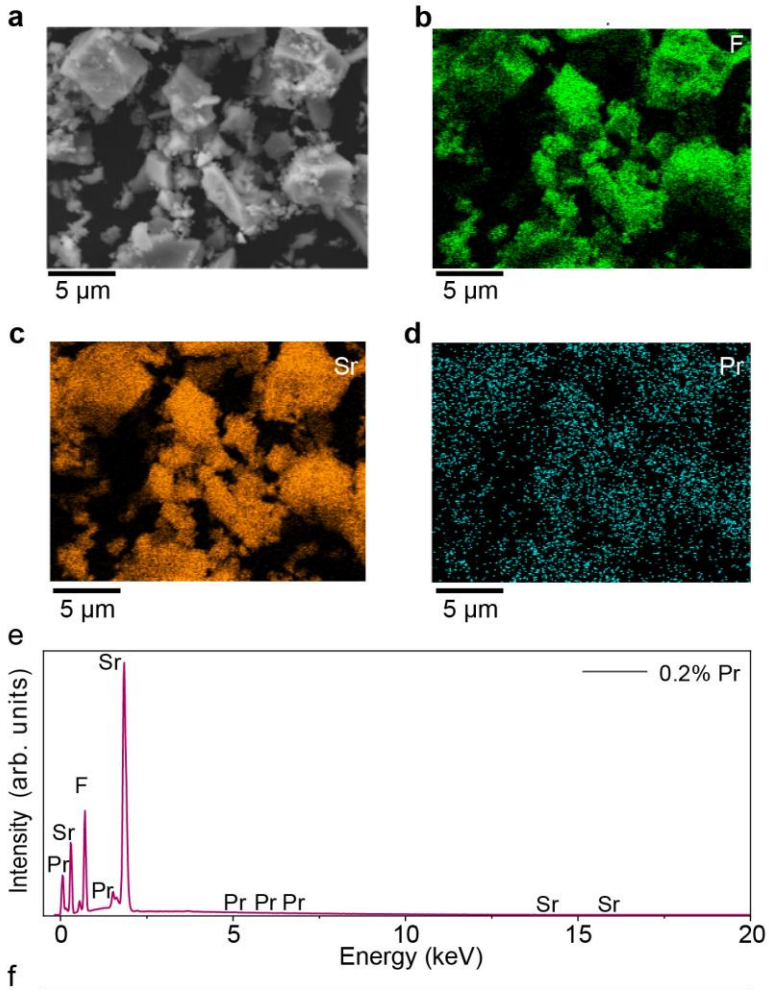

f

Element	Signal type	Weight %	Atomic %	Error % (Weight %)
F	EDS	29.75	66.16	0.15
Sr	EDS	70.02	33.77	0.18
Pr	EDS	0.23	0.07	0.17

Supplementary Fig. 4. (a) SEM image, (b) F, (c) Sr, and (d) Pr elemental mappings, (e) EDS spectrum and (f) Elemental analysis data of SrF_2:0.2%Pr^{3+}.

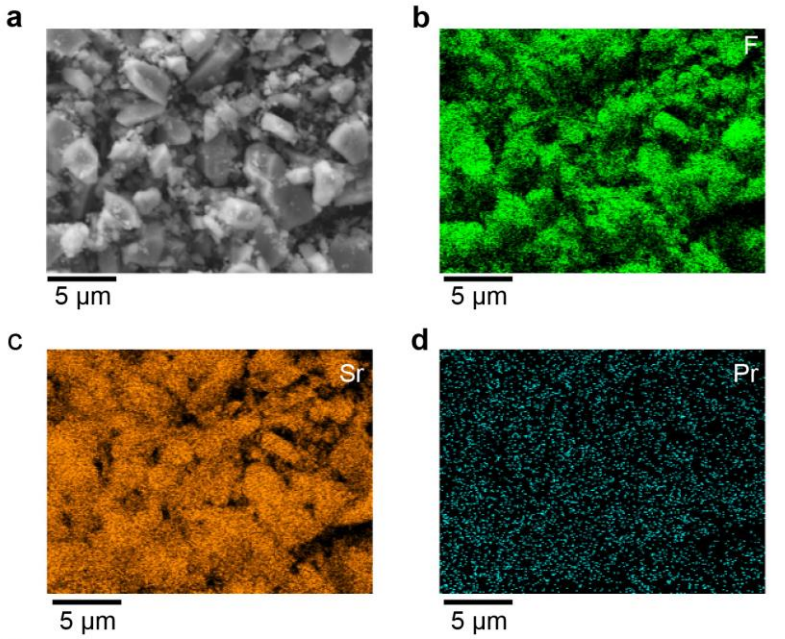

f

Element	Signal type	Weight %	Atomic %	Error % (Weight %)
F	EDS	30.43	66.93	0.14
Sr	EDS	69.01	32.91	0.17
Pr	EDS	0.56	0.16	0.15

Supplementary Fig. 5. (a) SEM image, (b) F, (c) Sr, and (d) Pr elemental mappings, (e) EDS spectrum and (f) Elemental analysis data of SrF_2:0.5%Pr^{3+}.

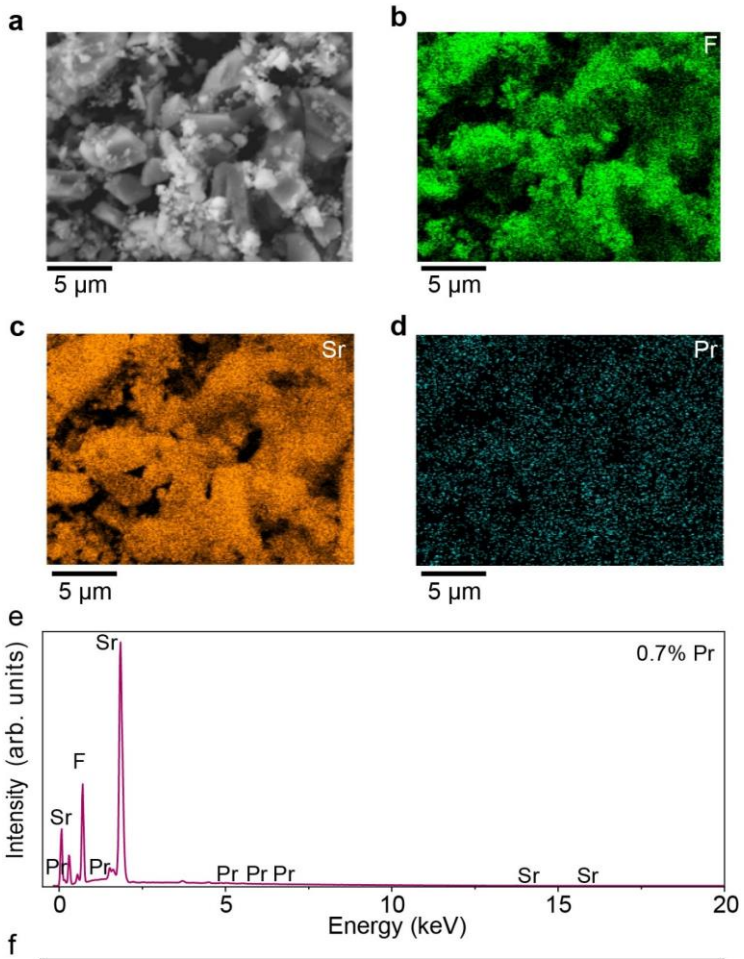

f

Element	Signal type	Weight %	Atomic %	Error % (Weight %)
F	EDS	30.02	66.52	0.12
Sr	EDS	69.19	33.24	0.15
Pr	EDS	0.79	0.24	0.14

Supplementary Fig. 6. (a) SEM image, (b) F, (c) Sr, and (d) Pr elemental mappings, (e) EDS spectrum and (f) Elemental analysis data of SrF_2:0.7%Pr^{3+}.

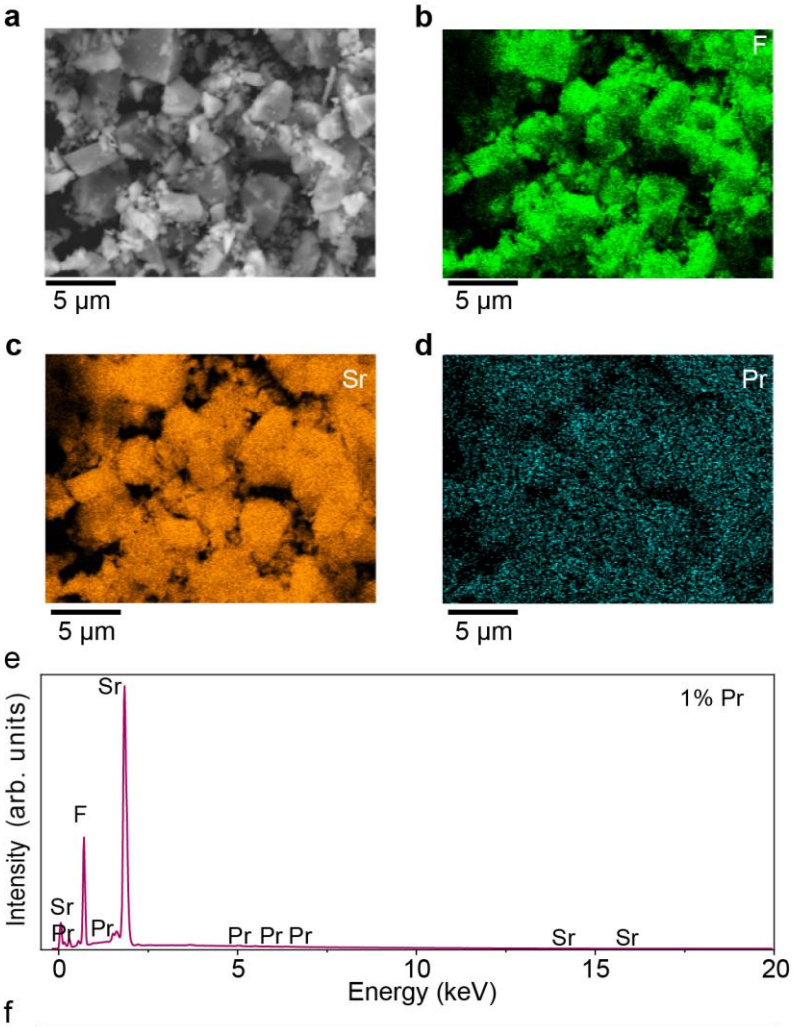

f

Element	Signal type	Weight %	Atomic %	Error % (Weight %)
F	EDS	29.47	65.97	0.08
Sr	EDS	69.39	33.68	0.09
Pr	EDS	1.14	0.34	0.08

Supplementary Fig. 7. (a) SEM image, (b) F, (c) Sr, and (d) Pr elemental mappings, (e) EDS spectrum and (f) Elemental analysis data of SrF_2:1%Pr^{3+}.

Comment 3: They mention that the materials prepared in this work exhibits the widest spectral range reported so far. A more comprehensive comparison with the existing ML materials is necessary to highlight the advancements made.

Response:

We greatly appreciate the comment. According to the comment, the original Fig. 1 had been redrawn as shown below (Supplementary Fig. 1) to provide a more comprehensive comparison with the existing ML systems, including lanthanides-doped SrZnOS, $Sr_3Al_2O_5Cl_2$, $CaGa_4O_7$, $Ca_2B_2O_5$, Y_2O_2S, CaZnOS, $SrAl_2O_4$, MgF_2, $NaYF_4$, $Sr_2P_2O_7$ and $Cs_2NaScCl_6$. For example, the ML wavelength of $CaGa_4O_7$:Ln (Ln= Tm^{3+}, Eu^{3+}, Sm^{3+}, Dy^{3+}, Er^{3+}, Tb^{3+} and Pr^{3+}) systems ranged from ≈420 to 910 nm, which was marked by a double-headed arrow segment of a certain width. By careful selection of different lanthanides or lanthanides pairs in single CaZnOS, the ML can be achieved over the ≈380–1540 nm range. This raises the question of how broad the wavelength range of ML can reach in a

single host. As shown in Supplementary Fig. 1, our work sets a new record in the shortwave limit (222 nm) and expands the available ML wavelength to the nearly whole 200–1700 nm range (short wave peak limit: 222 nm, long wave peak limit: 1620 nm). In addition to Supplementary Fig. 1, we also summarized Supplementary Table 1 to highlight the advancements made in this work. This table has been added to the Supplementary Information as Supplementary Table 1.

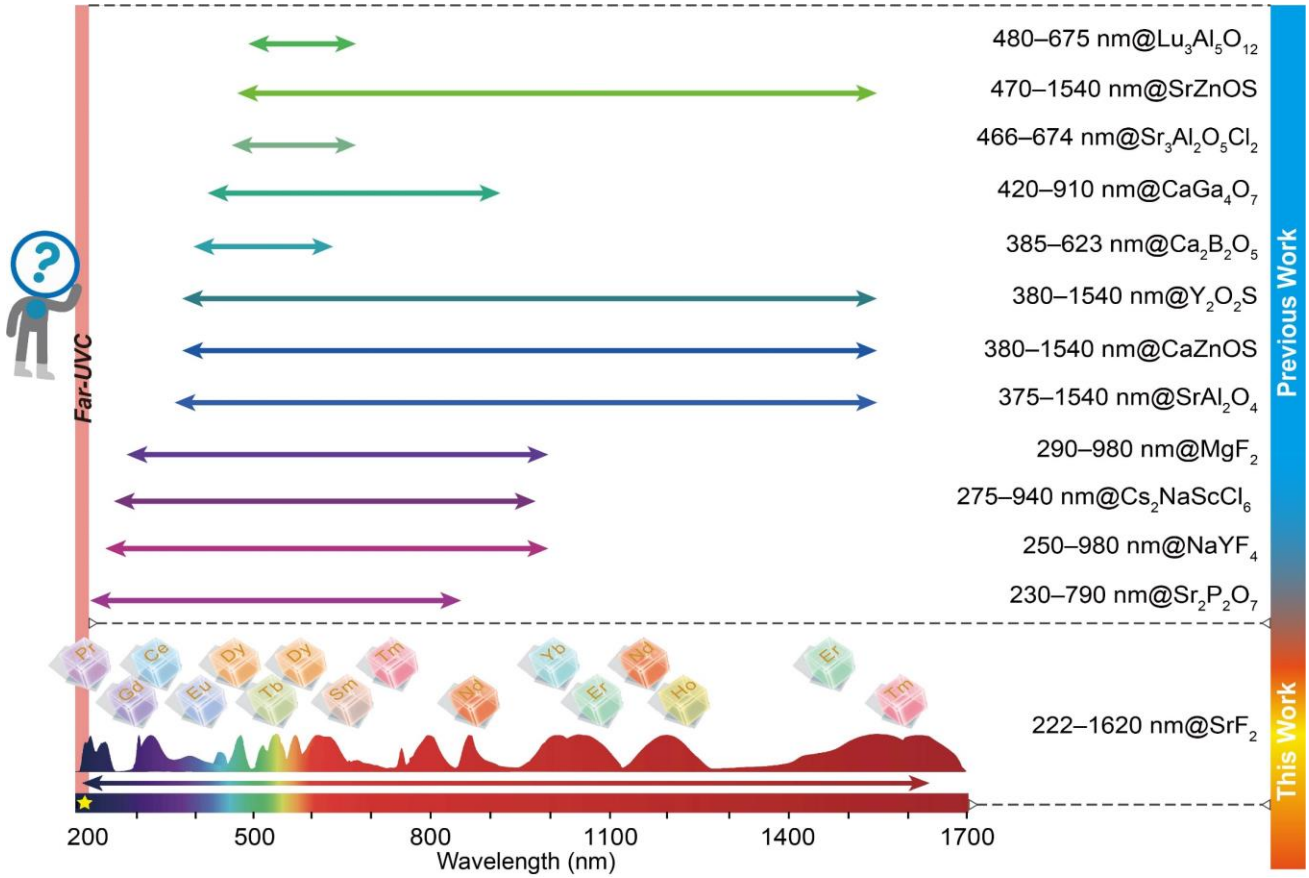

Supplementary Fig. 1. Comparison of ML spectral coverage of SrF_2 doped with lanthanides to previously reported systems.

Supplementary Table 1. Comparison of ML spectral coverage of SrF_2 doped with different lanthanides to previously reported systems.

Matrix	Doped ion	Emission band (nm)	References
CaZnOS	Mn^{2+}, Cu^{+}/Cu^{+}, Bi^{3+}, Sb^{3+}, Ce^{3+}, Pr^{3+}, Nd^{3+}, Sm^{3+}, Eu^{3+}, Tb^{3+}, Dy^{3+}, Ho^{3+}, Er^{3+}, Tm^{3+}, Yb^{3+}	380–1540	1, 2, 3, 4, 5, 6
SrZnOS	Mn^{2+}, Pr^{3+}, Nd^{3+}, Sm^{3+}, Tb^{3+}, Dy^{3+}, Ho^{3+}, Er^{3+}, Tm^{3+}, Yb^{3+}	420–1540	7
Y_2O_2S	Pr^{3+}, Nd^{3+}, Sm^{3+}, Tb^{3+}, Dy^{3+}, Ho^{3+}, Er^{3+}, Tm^{3+}, Yb^{3+}	480–1540	8, 9
Lu_2O_2S	Eu^{3+}	540–705	8
La_2O_2S	Eu^{3+}	615–705	8
Gd_2O_2S	Eu^{3+}	615–705	8
(Zn,Cd)S	Mn^{2+}, Ag, Au, Cu^{2+}	430–620	10
BaZnOS	Mn^{2+}, Bi^{3+}	480–630	11, 12
ZnS	Cu^{2+}, Mn^{2+}, Ag^{+}/Co^{2+}, Al^{3+}/Cu^{2+}, Mn^{2+}/Te^{2+}	456–648	13, 14, 15, 16

MgF_2	Mn^{2+}, Tm^{3+}, Yb^{3+}/Yb^{2+}, Dy^{3+}, Tb^{3+}, Eu^{3+}/Eu^{2+}, Sm^{3+}, Er^{3+}, Ho^{3+}	280–1000	17, 18, 19, 20
$KMgF_3$	Tb^{3+}	494–621	21
CaF_2	Tb^{3+}, Sm^{3+}, $Ce^{3+,}$ $Tm^{3+,}$ Eu^{3+}	425–825	22, 23
$NaYF_4$	Pr^{3+}, Sm^{3+}, Tb^{3+}, Dy^{3+}, Ho^{3+}, Er^{3+}, Tm^{3+}	250–980	24, 25, 26
$NaLuF_4$	$Tb^{3+,}$ Ho^{3+}	486–647	27, 28
ZnF_2/ZnO	Mn^{2+}	585	29
$NaLuF_4$	Ho^{3+}	486–647	28
$NaCa_2GeO_4F$	Mn^{2+}	570	30
$Sr_3(Al,Ga)O_4F$	Eu^{3+}, Tb^{3+}	488–704	31
Cs_2ZrCl_6	Te^{4+}	576	32
$CaCl_2$	Eu^{2+}	432	33
$NaCl$	Eu^{2+}	480	34
$Sr_5(PO_4)_3Cl$	Eu^{2+}	455	35
$Sr_3Al_2O_5Cl_2$	Dy^{3+}, Eu^{2+}, Tb^{3+}, Ce^{3+}, Tm^{3+}/Eu^{3+}	466–674	36, 37, 38
$Sr_5(PO_4)_3(F,Cl,Br)$	Eu^{3+}/Eu^{2+}	446–700	39
$Sr_5(PO_4)_3Cl$	Eu^{2+}, Mn^{2+}	400–700	40
$Cs_2NaScCl_6$	Sb^{3+}, Pr^{3+}, Nd^{3+}, Sm^{3+}, Tb^{3+}, Dy^{3+}, Ho^{3+}, Er^{3+}, Tm^{3+}, Yb^{3+}, Gd^{3+}, Ce^{3+}, Ag^{+}/Bi^{3+} Mn^{2+}	275–940	41
Cs_2HfCl_6	Te^{4+}	557	42
$Ca_6BaP_4O_{17}$	Ce^{3+}	488	43
$Ca_9Bi(PO_4)_7$	Ce^{3+}, Bi^{2+}	358-682	44
$SrMg_2(PO_4)_2$	Eu^{2+}, Eu^{2+}/Mn^{2+}	412–673	45, 46, 47
$CaZr(PO_4)_2$	Eu^{2+}	474	48, 49, 50
$Sr_8MgCe(PO_4)_7$	Tb^{3+}/Mn^{2+}	488–620	51
$Ca_6BaP_4O_{17}$	Eu^{2+}	540	52
$Ca_9Al(PO_4)_7$	Tb^{3+}, Mn^{2+}	480–648	53
$Sr_2P_2O_7$	Pr^{3+}, Tb^{3+}, Dy^{3+}, Sm^{3+}, Eu^{2+}, Ce^{3+}, Sn^{2+}, Mn^{2+}	230–800	54, 55
$Ca_9Al(PO_4)_7$	Ce^{3+}	300–800	56
$Ca_9NaMg(PO_4)_7$	Tb^{3+}	415–624	57
$SrAl_2O_4$	Eu^{2+}/Dy^{3+}, Ce^{3+}/Ho^{2+}, Eu^{2+}/Er^{3+}, $Eu^{2+}/Cr^{3+}/Nd^{3+}$, Ce^{3+}, Eu^{2+}, Nd^{3+}/Eu^{2+}, Er^{3+}/Eu^{2+}, Ce^{3+}/Ho^{3+}	375–1540	58
$LaAlO_3$	Cr^{3+}	685–750	59
$Lu_3Al_5O_{12}$	Ce^{3+}, Pr^{3+}, $Eu^{3+/2+}$, Tb^{3+}, Sm^{3+}, Ho^{3+}, Dy^{3+}, Er^{3+}, Nd^{3+}, Tm^{3+}	480–675	60
$Y_3Al_5O_{12}$	Ce^{3+}, Cr^{3+}	560–688	61, 62
$CaYAl_3O_7$	Eu^{2+}, Ce^{3+}	421–440	63, 64
$ZnAl_2O_4$	Mn^{2+}	512	65
$SrMgAl_{10}O_{17}$	Ce^{3+}	480	66
$SrMgAl_6O_{11}$	Eu^{2+}	512	67
$BaMgAl_{12}O_{17}$	Eu^{2+}	450	68
$CaLaAl_3O_7$	Tb^{3+}	411–622	69
$BaLaAl_3O_7$	Eu^{3+}	595–615	70
$CaGa_4O_7$	Pr^{3+}, Tb^{3+}, Er^{3+}, Dy^{3+}, Mn^{2+}, Sm^{3+}, Eu^{3+}, Tm^{3+}, Nd^{3+}	420–910	71, 72
$Ca_5Ga_6O_{14}$	Tb^{3+}	484–625	73
$Y_3Ga_5O_{12}$	Tb^{3+}	380–690	74
$MgGa_2O_4$	Mn^{2+}, Cr^{3+}, Bi^{3+}, Pr^{3+}	480–770	75, 76, 77, 78
$Ca_3Ga_4O_9$	Tb^{3+}, Eu^{3+}	380–701	79, 80

$SrGa_{12}O_{19}$	Cr^{3+}, Cr^{3+}/Pr^{3+}	710–750	81, 82, 83
$Y_3Al_2Ga_3O_{12}$	Gd^{3+}	310	84
$Lu_3Al_2Ga_3O_{12}$	Cr^{3+}, Tb^{3+}	380–706	85, 86
$Y_3Al_3Ga_2O_{12}$	Ce^{3+}	528	87
$CaSrGa_4O_8$	Tb^{3+}	480–630	88
Y_3GaO_6	Tb^{3+}	484–590	89
$LiGa_5O_8$	Matrix, Cr^{3+}, Pr^{3+}	525–716	81, 90, 91
$LiGaO_2$	Fe^{3+}, Mn^{2+}	660–750	92, 93
$ZnGa_2O_4$	Mn^{2+}, Cr^{3+}	505–692	75, 94
$Lu_3Al_2Ga_3O_{12}$	Tb^{3+}, Eu^{3+}	383–709	95
$(Li,Na)_2(Zn,Mg)GeO_4$	Mn^{2+}	515–535	96
$Zn_3Ga_2GeO_8$	Cr^{3+}	700	81
$CaZnGe_2O_6$	Mn^{2+}	676	97, 98
$Ca_2YGa_3Ge_2O_{12}$	Cr^{3+}/Nd^{3+}	767–1340	99
$Mg_3Ga_2GeO_8$	Cr^{3+}	650–1000	100
$MgGeO_3$	Mn^{2+}	691	101
$CaMgGe_2O_6$	Mn^{2+}	670	102
$Zn_2(Ge_{0.9}Si_{0.1})O_4$	Mn^{2+}	535	103
Na_2ZnSiO_4	Mn^{2+}	514	96
$Sr_2MgSi_2O_7$	Eu^{2+}/Dy^{3+}, Eu^{2+}	460–580	104, 105
$Ca_2MgSi_2O_7$	Eu^{2+}	545	106
$Ca_2Al_2SiO_7$	Ce^{3+}	400	107
$Sr(Ba,Ca,Sr)MgSi_2O_7$	Eu^{2+}	450–490	108
$(Ca,Sr)Al_2Si_2O_8$	Eu^{2+}	403–428	109
$(Ca,Sr)_8Mg_3Al_2Si_7O_8$	Ce^{3+}	500–800	110
$Ca_2Ga_2SiO_7$	Tb^{3+}	495–620	111
$Y_3Ga_3MgSiO_{12}$	Cr^{3+}	731	112
$CaNb_2O_6$	Pr^{3+}	613	113
$Ca_2Nb_2O_7$	Pr^{3+}	613	113
$Ca_3Nb_2O_8$	Pr^{3+}	613	113
$Sr_2Nb_2O_7$	Pr^{3+}	613	114
$NaNbO_3$	Pr^{3+}/Er^{3+}	613	115
$LiNbO_3$	Pr^{3+}, Nd^{3+}	619–895	116, 117
$(Na,Mg)NbO_3$	Pr^{3+}	613	118
$LiTaO_3$	Tb^{3+}, Pr^{3+}/Gd^{3+}	510–692	119, 120
$(Ba,Ca)TiO_3$	Pr^{3+}	613	121, 122, 123
$Sr_3Sn_2O_7$	Sm^{3+}, Nd^{3+}, Nd^{3+}/Yb^{3+}	570–1340	124, 125, 126, 127, 128, 129, 130
Sr_2SnO_4	Sm^{3+}	574–745	131
$SrZn_2S_2O$	Mn^{2+}	610	132
ZrO_2	Sm^{3+}, Ti^{4+}	478–614	133, 134
Ga_2O_3	Cr^{3+}/In^{3+}	715–830	135
$BaSi_2O_2N_2$	Eu^{2+}	500	8
$Ba_{0.5}Sr_{0.5}Si_2O_2N_2$	Eu^{2+}	505	61
B_2O_3-SiO_2-ZnO	Tb^{3+}, Tm^{3+}, Eu^{3+}	455–710	136
$Ca_2B_2O_5$	Tb^{3+}, Dy^{3+}, Sm^{3+}, Eu^{3+}, Ce^{3+}	385–623	137
$(Sr,Ba)_2(Ga,Sc)SbO_6$	Cr^{3+}	830–1010	138
$BaSi_2O_2N_2$	Eu^{2+}	498	139
ZnB_2O_4	Mn^{2+}	550	140

Comment 4: The paper discusses the trap-controlled ML mechanism but lacks detailed experimental verification. To strengthen the proposed mechanism, the authors should incorporate time-resolved luminescence or other dynamic studies to provide further evidence.

Response:

We greatly appreciate the comment. As proposed, time-resolved luminescence is a very important technology for investigating the dynamic mechanism of optical phenomenon. In the field of ML, there is only one paper reporting on time-resolved process of ML (*Adv. Funct. Mater.* 2023, 33, 2304917), to the best of our knowledge. In this milestone work, the authors revealed the intrinsic decay of ML, aiming to achieve ultrafast-response stress sensing.

By using a similar technology, we measured the PL (λ_{ex}=440 nm, λ_{em}=488 nm) and trap-controlled ML decay curves of SrF_2:0.5%Pr^{3+}. In order to facilitate comparison, these two decay curves are plotted in Supplementary Fig. 34. By using the single-exponential function, the intrinsic lifetime of PL was fitted to 239 μs, a typical value of the lifetime of 4f→4f transition of Pr^{3+}. When the dynamic force was no longer applied to the sample, the trap-controlled ML continued for over 137 ms, three orders of magnitude larger than that of PL. It suggests that the processes of PL and trap-controlled ML are totally different for SrF_2:0.5%Pr^{3+}. As trap-controlled ML involves the release and migration of charge carriers, it lasts significantly longer than the PL process. Therefore, such fact could also be regarded as indirect evidence that the defects indeed participated in the trap-controlled ML.

In the 'Mechanistic investigation of multi-stimulated emission' part of 'Results' section, we have added the following sentences, 'To gain insight into the trap-controlled ML mechanism after X-ray charging, we measured the PL (λ_{ex}=440 nm, λ_{em}=488 nm) and ML decay curves of SrF_2:0.5%Pr^{3+} (Supplementary Fig. 34). The results reveal that the duration time of ML is three orders of magnitude larger than that of PL. The observation supports the trap-controlled nature of the ML behavior, which involves the release and migration of charge carriers, thus taking a significantly longer time than PL (Supplementary Fig. 35).'. Please see these changes on page 10 in the revised manuscript. Moreover, we have added the measurement details of ML and PL lifetimes into the 'Methods' section. Please see them on page 16 in the revised manuscript.

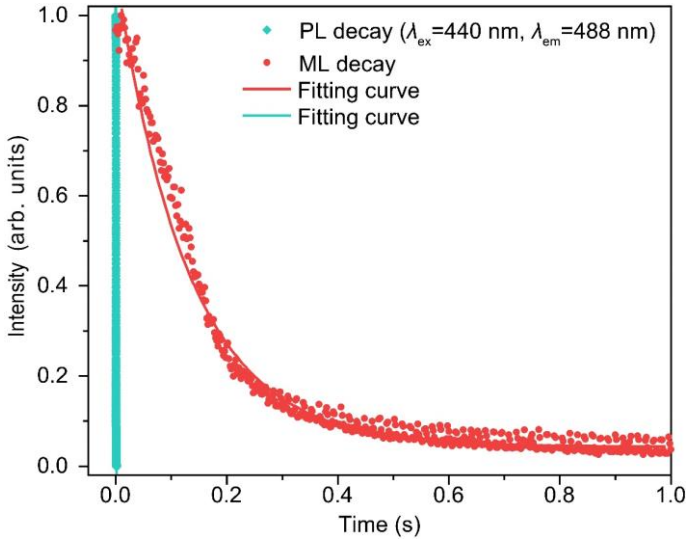

Supplementary Fig. 34. Decay curves of PL (λ_{ex}=440 nm, λ_{em}=488 nm) and trap-controlled ML of SrF_2:0.5%Pr^{3+}.

Comment 5: Although the role of X-ray pre-charging in enhancing ML is mentioned, the underlying processes remain insufficiently explored. It would be helpful for the authors to elaborate on how X-ray exposure specifically influences the charge trap states within the material and how these trapped charge carriers contribute to the enhanced ML. To further clarify the mechanism, the authors may

consider adding theoretical calculations of relevant energy bands and defect states to provide a more comprehensive understanding of the processes involved.

Response:

We greatly appreciate the comment.

(1) We conducted relevant experiments to verify how X-ray exposure specifically influences the charge trap states within the material. As shown in Supplementary Fig. 36, the TL intensity was gradually increased by extending the X-ray pre-charging time, approaching almost saturation after 20 min of irradiation. These discussions suggested that the role of X-ray exposure was to boost the trapped carrier density.

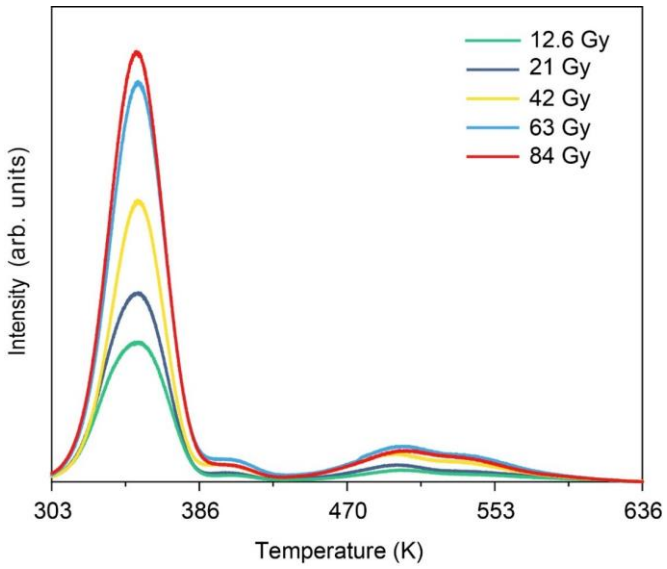

Supplementary Fig. 36. TL curves of SrF_2:0.5%Pr^{3+} after being charged by X-ray of different doses.

(2) Immediately afterwards, we performed the related experiments to demonstrate how the trapped charge carriers contributed to the enhanced ML. As shown in Fig. 4(e), the ML spectra were gradually increased by extending the X-ray pre-charging time, very similar to the case of TL curves shown in Supplementary Fig. 36. We then integrated the ML intensity and plotted it as a function of irradiation dose. As presented in Fig. 4(f), the ML and TL intensities had the same dependence on the irradiation dose, substantiating that the trapped charge carriers contributed to the enhanced ML.

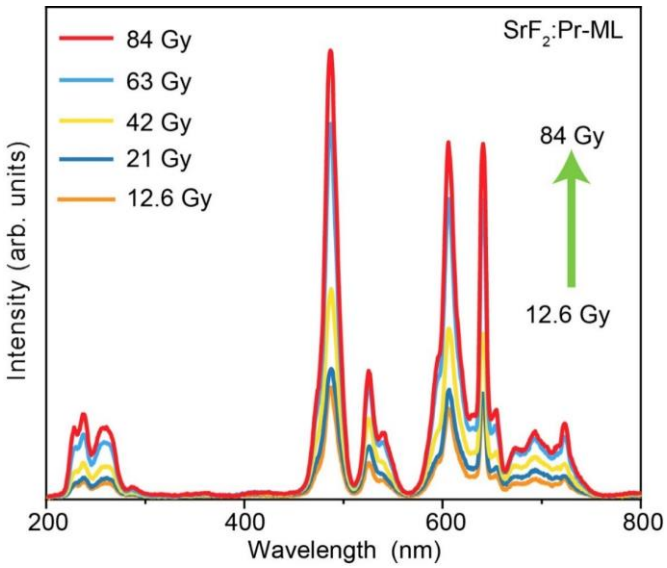

Fig. 4(e). ML spectra of SrF_2:0.5%Pr^{3+} after different X-ray exposure dose.

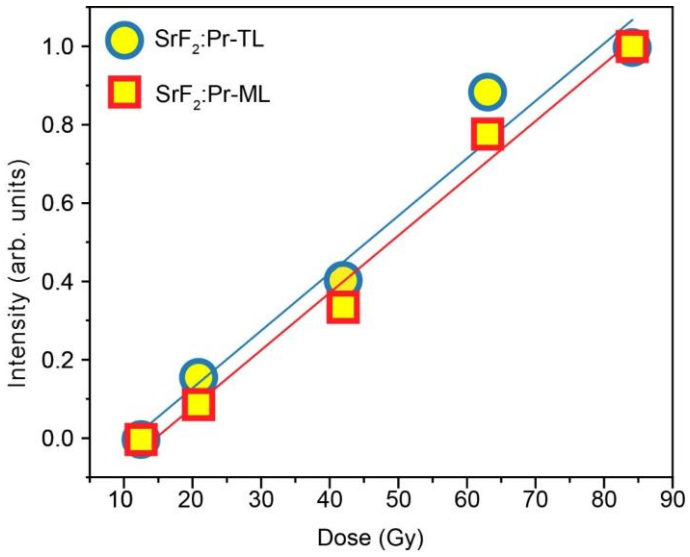

Fig. 4(f). Normalized TL and ML intensities of SrF_2:0.5%Pr^{3+} as a function of X-ray irradiation dose.

In the 'Mechanistic investigation of multi-stimulated emission' part of 'Results' section, we have added the following sentences, 'To shed more light on the multi-stimulated luminescence, the trapped charge carriers were adjusted by regulating the X-ray dose. With the increase of charging time, the ML intensified gradually (Fig. 4e). The observation is as anticipated due to the increased population in trap states, as confirmed by TL measurement (Supplementary Fig. 36). After performing the integral calculation, we clearly demonstrated the positive correlation of ML and TL intensities (Fig. 4f). As PersL is also closely related to TL, it is not difficult to understand that the stronger the PersL, the stronger the ML typically is (Supplementary Figs. 37 and 38). These observations provided additional evidence that the PersL and ML originated from the same trapped charge carriers.'. Please see these changes on page 11 in the revised manuscript.

(3) According to your suggestion, we have added theoretical calculations to explain the relevant energy bands and defect states to provide a more comprehensive understanding of the processes involved. In SrF_2, Sr ions adopt a +2 valence state. When trivalent Tb^{3+} ions are introduced to substitute Sr^{2+} lattice sites, charge imbalance arises. Taking 6.25% Pr^{3+} doping as an example, two primary charge compensation mechanisms exist: (1) Two Tb^{3+} ions substituting two Sr^{2+} ions introduce +2 excess charge, with charge neutrality maintained by the creation of one Sr vacancy, described as $2[Tb_{Sr}]^{+} + [V_{Sr}]^{2-}$ (Supplementary Fig. 42a). (2) Alternatively, two Tb^{3+} ions substituting two Sr^{2+} ions require the simultaneous formation of two F vacancies and two Sr vacancies for charge balance, expressed as $2[Tb_{Sr}]^{+} + 2[V_F]^{+} + 2[V_{Sr}]^{2-}$ (Supplementary Fig. 42b). Supplementary Table 5 presents the cell (E_{coh}) corresponding to different defects within the SrF_2 crystal. The definition of E_{coh} is as follows: $E_{coh} = (E_s - a \times E_{Sr} - b \times E_F - c \times E_{Pr})/N$. Here, E_s represents the total energy of the supercell. E_{Sr}, E_F and E_{Pr} are the free state energies of the Sr, F and Pr atoms, respectively. a, b and c denote the numbers of the corresponding atomic species in the supercell, and N is the total number of atoms in the supercell. The results indicate that the atomic E_{coh} (-5.44 eV) for the $2[Pr_{Sr}]^{+}+[V_{Sr}]^{2-}$ defect cluster is the smallest. It means that two Pr^{3+} dopants would replace two Sr^{2+} cations in the SrF_2 crystal, resulting in one Sr^{2+} vacancy to keep the charge balance in the SrF_2 crystal. In addition, fluorine vacancies and interstitials were expected to be generated in the fluorides under X-ray irradiation, according to previous reports (*Nature* 2021, 590, 410; *Nat. Commun.* 2022, 13, 5739). Therefore, there were abundant defects in SrF_2:Pr^{3+} to trap charge carriers.

In the 'Mechanistic investigation of multi-stimulated emission' part of 'Results' section, we have added the following sentences, 'Our theoretical calculations (Supplementary Fig. 42 and Table 5) suggest that the substitution of two Pr^{3+} ions for two Sr^{2+} sites most likely occurred, resulting in one consequent Sr^{2+} vacancy. Moreover, fluorine vacancies and interstitials were expected to be

generated in the fluorides under X-ray irradiation according to previous reports. Therefore, there were abundant defects in $SrF_2:Pr^{3+}$ to trap charge carriers[64–66].'. Please see these changes on page 12 in the revised manuscript.

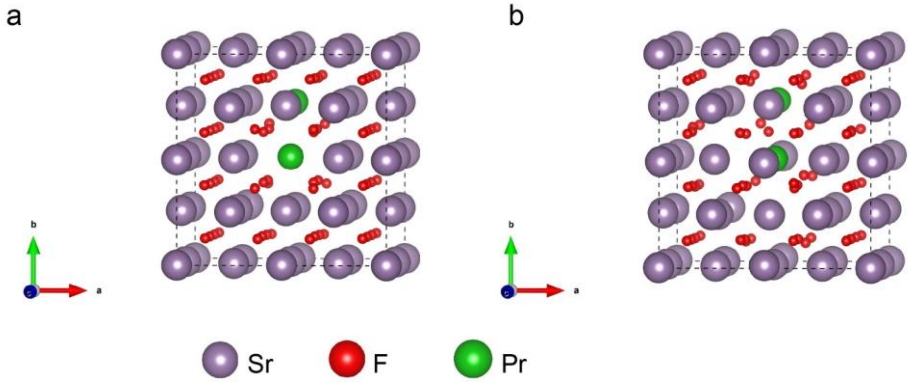

Supplementary Fig. 42. **Charge compensation mechanisms**. Two specific kinds of defects in SrF_2 crystal, including Tb^{3+} replacing Sr^{2+} $[Tb_{Sr}]^+$, Sr vacancy $[V_{Sr}]^{2-}$ and F vacancy $[V_F]^+$, taking 6.25% Pr^{3+} doping as an example. **a** Two Tb^{3+} ions substituting for two Sr^{2+} ions, with charge neutrality maintained by the creation of one Sr vacancy, described as $2[Tb_{Sr}]^+ + [V_{Sr}]^{2-}$. **b** Two Tb^{3+} ions substituting for two Sr^{2+} ions, with charge neutrality maintained by the simultaneous formation of two F vacancies and two Sr vacancies, expressed as $2[Tb_{Sr}]^+ + 2[V_F]^+ + 2[V_{Sr}]^{2-}$.

Supplementary Table 5. DFT calculated cohesive energies (E_{coh}) for the different defects in the SrF_2 crystal, including $2[Pr_{Sr}]^+ + [V_{Sr}]^{2-}$ and $2[Tb_{Sr}]^+ + 2[V_F]^+ + 2[V_{Sr}]^{2-}$.

Defects	Number of atoms (N)	Supercell E_s (eV)	free state energy (eV)			Cohesive energies E_{coh} (eV)
			E_{Sr}	E_F	E_{Pr}	
$2[Pr_{Sr}]^+ + [V_{Sr}]^{2-}$	95	-546.93	-0.02	-0.45	-0.19	-5.44
$2[Tb_{Sr}]^+ + 2[V_F]^+ + 2[V_{Sr}]^{2-}$	92	-526.90	-0.02	-0.45	-0.19	-5.41

Comment 6: The authors should provide additional ML data to further substantiate the self-recovering ML features of $SrF_2:Pr^{3+}$. And they should also add a comparison of the ML intensity before and after each cycle multiple cycles.

Response:

We greatly appreciate the comment. According to your suggestion, we examined the repeatability of self-recoverable ML. For self-recoverable ML, its intensity decreased after several cycles of continuous operation, as shown in Supplementary Fig. 11(a). This phenomenon had also been previously observed by several groups for self-recoverable ML systems. We checked the XRD results of $SrF_2:0.5\%Pr^{3+}$ that had been continuously ground, and found no change in crystal structure (Supplementary Fig. 12). The comparison of SEM images of $SrF_2:Pr^{3+}$ before and after grinding suggested the samples became progressively finer (Supplementary Fig. 13). As the surface area and morphology of samples had been modified, it was reasonable to assume that the self-recovering ML property was affected to some extent.

In the 'Multi-stimulated far-UVC luminescence' part of 'Results' section, we have added the following sentences, "We next examined the repeatability of ML. Both the self-recoverable and trap-controlled ML decreased after several cycles of continuous operation (Fig. 3c, Supplementary Fig.

11). This phenomenon was also previously observed by several groups. By checking the XRD results of SrF_2:0.5%Pr^{3+} after grinding, we found no noticeable change in the crystal structure (Supplementary Fig. 12). The comparison of SEM images of SrF_2:Pr^{3+} before and after grinding suggested that the samples became progressively finer (Supplementary Fig. 13). As the surface area and morphology of samples had been modified, it was reasonable to assume that the ML property, including both self-recoverable and trap-controlled ML, were affected to some extent[60]." Please see these changes on page 8 in the revised manuscript.

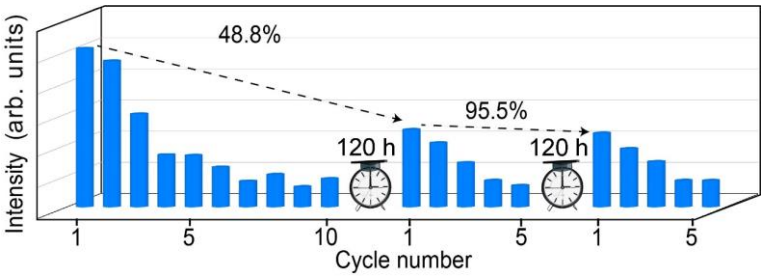

Supplementary Fig. 11(a). Repeatability test results of self-recoverable ML of SrF_2:0.5%Pr^{3+}.

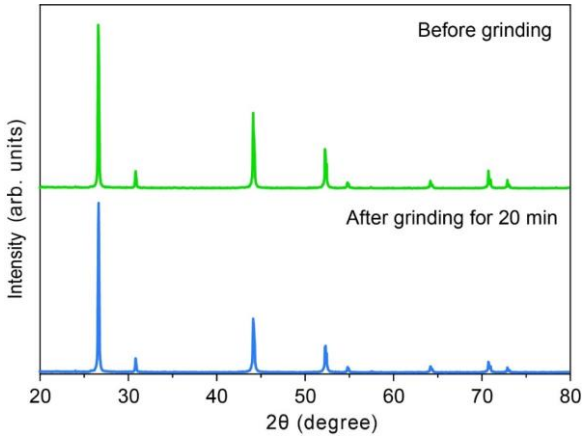

Supplementary Fig. 12. XRD patterns of SrF_2:0.5%Pr^{3+} before and after continuous grinding for 20 min.

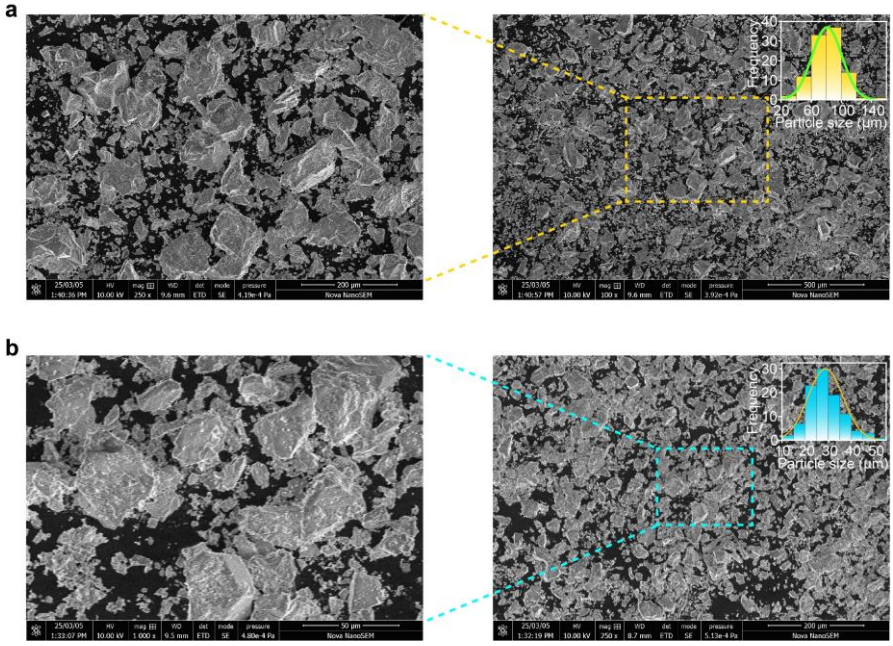

Supplementary Fig. 13. SEM images of SrF_2:0.5%Pr^{3+} **a** before and **b** after continuous grinding for 20 min.

Comment 7: Please confirm the accuracy of the description in line 194: "… leaving there many holes in the conduction band." Additionally, when using the abbreviation "PDMS" for the first time, the authors should provide the full form to ensure that readers unfamiliar with the abbreviation can easily understand it.

Response:

We sincerely apologize for this oversight and have revised these sentences. To avoid similar typos and grammatical errors, we have thoroughly checked the manuscript.

Moreover, we have examined the full text carefully to ensure that all abbreviations have been defined in full when used for the first time.

Reviewer #2:

This manuscript reports the mechanoluminescence of Ln-doped SrF_2, which is quite similar with the same authors' recent publications for ML in $NaYF_4:Pr^{3+}$ and $Sr_2P_2O_7:Pr^{3+}$. Besides the difference in host adopted, the authors try to highlight two innovations, i.e., the widest ML wavelength span (200 nm to 1700 nm) and the shortest ML wavelength (222 nm). In my opinion, however, these two points are far from enough to persuade ones to support the publication of the present work in Nature Communications, due to the following issues.

Response:

We appreciate the reviewer's critical feedback very much, which helps us rethink our article and improve the manuscript. There is an old saying in China: 'Teaching a man to fish is better than giving him a fish.' Originally, our intention was to 'give the readers a fish', but after hearing your advice, we decided to teach the readers 'how to fish'. By substantial revision, we believe that the manuscript can now provide a general approach for the readers to seek and design more materials that might have far-UVC ML in the future. Please see the following responses to your comments.

Comment 1: UVC MLs are observed for all three Pr^{3+} doped phosphors ($Sr_2P_2O_7$/$NaYF_4$/SrF_2). However, only the ML for $SrF_2:Pr^{3+}$ exhibits the transition of $4f5d\rightarrow{}^3H_4$ (222 nm). What is the origin for this difference? This question is crucial If the authors take "the shortest ML wavelength" so important. Unfortunately, the authors fail to give any explanation about it.

Response:

We greatly appreciate the critical comment.

First of all, 'the shortest ML wavelength' is an important highlight of our work. No one can deny that emission wavelength is one of the most important parameters for ML materials as it directly determines specific applications. Many research groups have made substantial efforts to expand available ML wavelengths, as summarized in Supplementary Fig. 1. However, scientists mainly focus on the visible and near-infrared regions, with little attention to the UV range. In fact, no more than ten articles have reported on the progress of UVC ML, among which none have reported on far-UVC ML. Considering the importance of far-UVC light, it is meaningful to explore the materials that are capable of emitting far-UVC ML.

We propose a set of guidelines for far-UVC emission design, as shown in Fig. 1.

(1) At the most basic level, the bandgap of the host where Pr^{3+} ions are embedded should be greater than 6.17 eV (≈200 nm), such that the far-UVC photons are not absorbed by the host (Fig. 1, step 1). This requirement excludes a large portion of semiconductors and oxysalts, such as sulfide (ZnS:3.5~3.8 eV, CaS:3.06 eV), oxides (Y_2O_3:5.5 eV, ZnO:3.37 eV and $BaTiO_3$:3.3 eV), tungstates ($CaWO_4$:4.5 eV) and molybdates ($CaMoO_4$:3.7 eV), despite their popularity in hosting visible emitting ions.

(2) Next, we pay attention to the $^1S_0$ state of Pr^{3+}, which may generate far-UVC emissions through the $^1S_0\rightarrow{}^3H_4$ (≈215 nm) and $^1S_0\rightarrow{}^3H_5$ (≈225 nm) transitions (Fig. 1, step 2). It should be noted, however, that the emission intensities of these intra-configurational transitions are very weak due to their parity-forbidden nature. Another downside is that the total transition branching ratios of $^1S_0\rightarrow{}^3H_{4,5}$ are less than 1%. More than 60%~80% of the excited $^1S_0$ state terminates in the lower-lying $^1I_6$ state, peaking at ≈400 nm[49, 50]. This explains why the $^1S_0\rightarrow{}^3H_4$ (≈215 nm) and $^1S_0\rightarrow{}^3H_5$ (≈225 nm) transitions are hardly observed in most reports. Even if they are observed under optimal conditions, the emission intensity is too weak[51, 52].

(3) The above discussions suggest that the $^1S_0$ state is unfavorable to far-UVC emissions. Therefore, it is more advisable to expect far-UVC emissions from the 4f5d state. The longwave boundary of far-UVC is at 230 nm, corresponding to ≈43478 cm^{-1}. Accordingly, the lower limit of the 4f5d state should be above 43478 cm^{-1} (Fig. 1, step 3). Under this premise constraint, the energy position of the 4f5d state should be as close as possible to the center wavelength (≈46500 cm^{-1}) of

far-UVC, ensuring that most emissions fall within the far-UVC range.

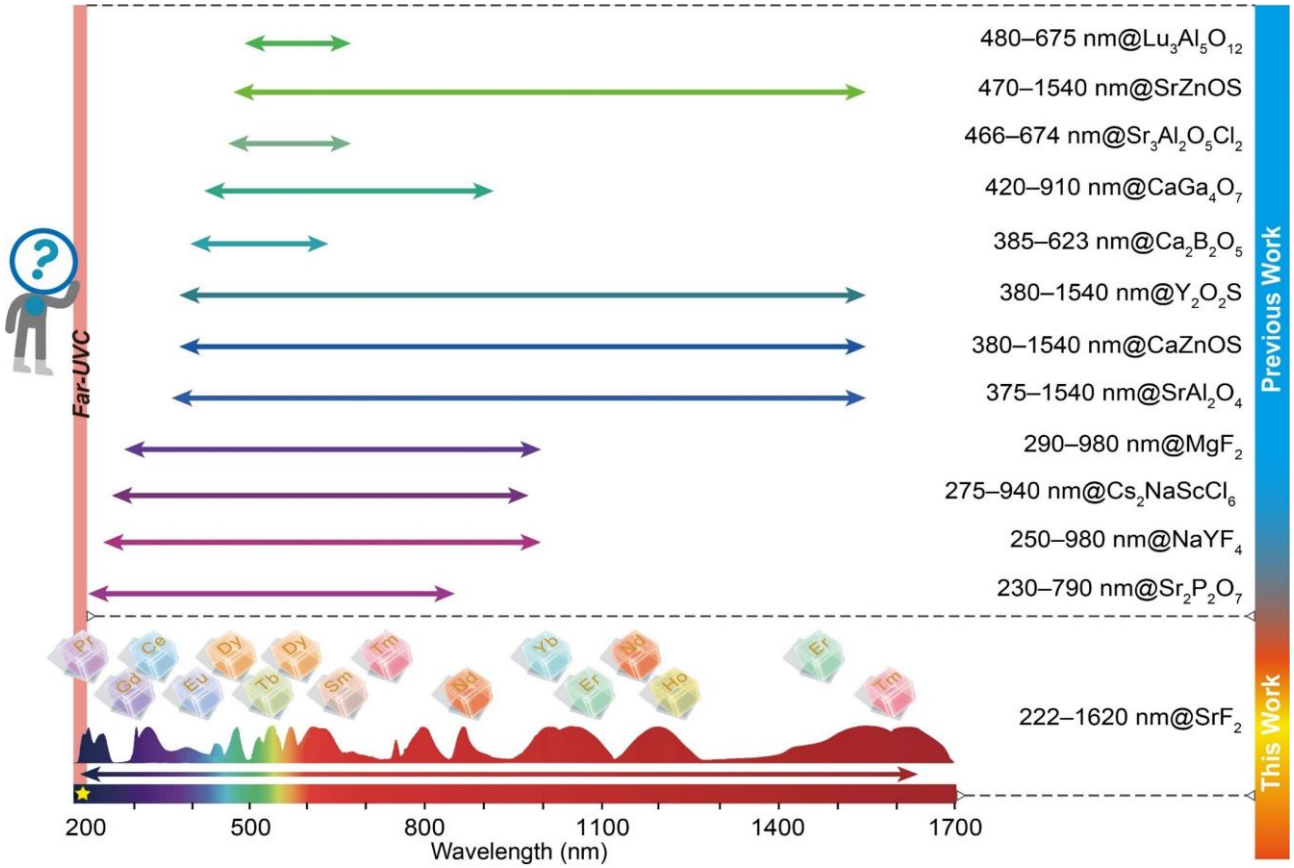

Supplementary Fig. 1. Comparison of ML spectral coverage of SrF_2 doped with lanthanides to previously reported systems.

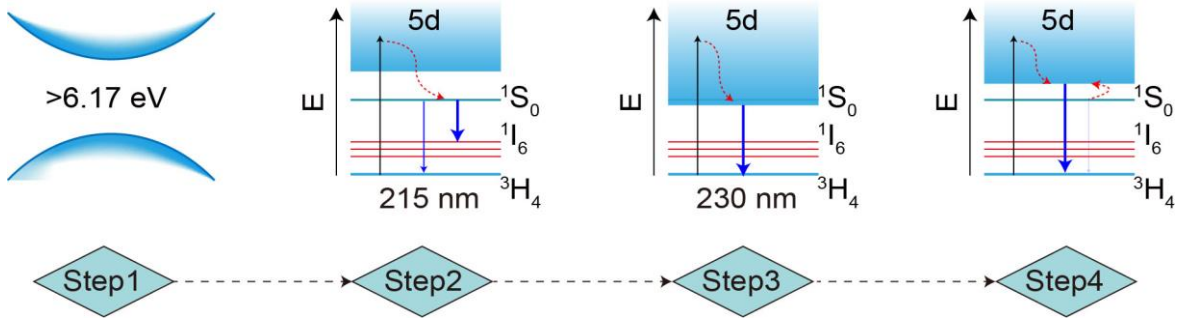

Fig. 1. Design principles for far-UVC emission. Step 1: Calculation of the band gap of the host crystal. Step 2: Assessment of the position and intensity of transitions from the $^1S_0$ state of Pr^{3+}. Step 3: Determine the lowest energy 4f5d state for far-UVC emission. Step 4: Analysis of the situation in which the transitions from the 4f5d state of Pr^{3+} dominate the emissions as well as the shortwave boundary of far-UVC.

(4) Notably, an over-high energy of the 4f5d should also be avoided. Otherwise, the excited electrons at the 4f5d state will be non-radiatively relaxed to the lower $^1S_0$ state, followed by the emissions from the $^1S_0$ state (Fig. 1, step 4). In $SrAl_{12}O_{19}:Pr^{3+}$, for example, the lowest 4f5d state and $^1S_0$ state were ≈47600 cm^{-1} and ≈46500 cm^{-1}, respectively, with an energy difference of 1100 cm^{-1} [53]. In this compound, only weak transitions from the $^1S_0$ state were observed over the far-UVC region at 220 nm. In contrast, the lowest 4f5d state in $LaB_3O_6:Pr^{3+}$ is higher than the $^1S_0$ state by ≈900 cm^{-1}, and the 5d→4f transitions dominated the emission spectrum in the far-UVC range due to the Boltzmann distribution between the $^1S_0$ state and the upper 4f5d state[54]. Combining the above two

situations, we suggest that the position of the 4f5d state should not be higher than that of the $^1S_0$ state by 1000 cm^{-1}.

Summarizing all the information above, we can draw the following semi-empirical conclusion: the 4f5d state of Pr^{3+} should be in the range of 43478 to 47500 cm^{-1}. Considering that the position of the $^1S_0$ state may slightly change with the alteration of the host (< 500 cm^{-1}), the upper energy limit of the 4f5d state of Pr^{3+} can be appropriately relaxed to ≈48000 cm^{-1}. Additionally, it is important to note that the host material where Pr^{3+} ions are embedded needs to have good far-UVC transmission. This clue points to fluorides that typically possess a wide band gap and good ultraviolet transmittance. Based on previous reports, the 4f→5d transition of Pr^{3+} in SrF_2 had an absorption peak at ≈46600 cm^{-1} [55]. Such energy value well satisfies the above guidelines, thus making it possible to achieve far-UVC ML. Therefore, $SrF_2:Pr^{3+}$ was chosen as a representative for examination in the subsequent sections.

All the above discussions have been added to the 'Design principles for far-UVC emission' part of 'Results' section. Please see these changes on pages 4–6 in the revised manuscript.

Comment 2: The wide ML wavelength span can be obtained by means of a serial of $Ln^{2+,3+}$ doping/co-doping, which is quite easy to conceive by anyone. I don't think this point is a remarkable achievement.

Response:

We greatly appreciate the critical comment.

(1) As mentioned, there is no literature reporting on far-UVC ML. Thus, we have shifted our focus to exploring far-UVC ML materials in the revised manuscript. After we achieve the first case of far-UVC ML, we can obtain the widest ML wavelength span in a single host matrix, which now becomes an added achievement of our investigation.

(2) However, it should be noted although it is relatively easy to expand the ML wavelength to the visible and near-infrared regions, achieving far-UVC ML was by no means an easy task. Let us see Supplementary Fig. 1 and take the commonly studied CaZnOS as an example. By careful selection of different lanthanides or lanthanides pairs in single CaZnOS, the ML can be achieved only over the 380–1540 nm range. What happens if we embed Pr^{3+} into CaZnOS? Researchers have long thought of such idea. However, not even UVA ML was detected, let alone the UVC band. The reason lies in the lack of suitable guidelines.

(3) To sum up, we respect your opinion by putting the wide ML wavelength span in second place to prioritize the far-UVC ML in the revised manuscript.

Comment 3: Why there is no UVC components for PersL (Fig.3b)?

Response:

We greatly appreciate the comments. We re-checked this figure and the original data to explain the phenomenon. The PersL spectrum in original Fig. 3b was obtained at 3 h after switching off the X-ray. The inset in the following Fig. R1 shows the enlarged UVC part, suggesting that the UVC PersL existed at this moment, but with a low signal-to-noise ratio. Supplementary Fig. 17 shows the PersL spectra of SrF_2:0.5%Pr^{3+} at different decay times. As the UVC PersL has a low initial intensity compared to the visible counterpart, it attenuates more quickly than visible light and decays to undetectable level first (Supplementary Fig. 16). To avoid ambiguity, we redrew this figure by putting the PersL spectrum obtained immediately after the stoppage of X-ray. As shown below in Fig. 3b, the UVC components of the PersL spectra are obvious to observe. Note that the ML spectrum in original Fig. 3b was obtained upon stimulation of external force at 25 N. In the updated Fig. 3b, it has been replaced by the spectrum collected at 5 N. Under such conditions, the UVC part has weakened a bit. This part has already been mentioned in the first edition of the manuscript. Please see them on pages 8 and 9 in the revised manuscript.

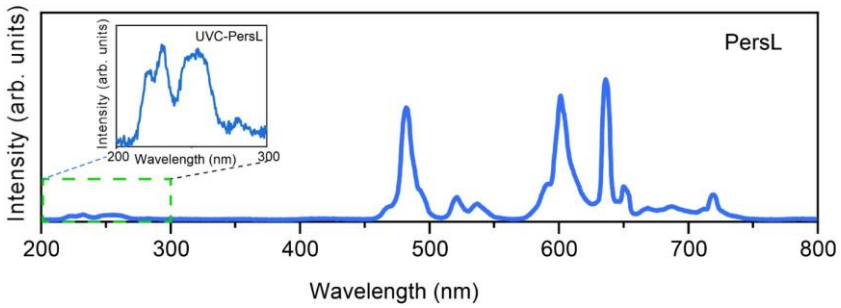

Fig. R1. PersL spectrum of SrF_2:0.5%Pr^{3+} at 3 h after switching off the X-ray.

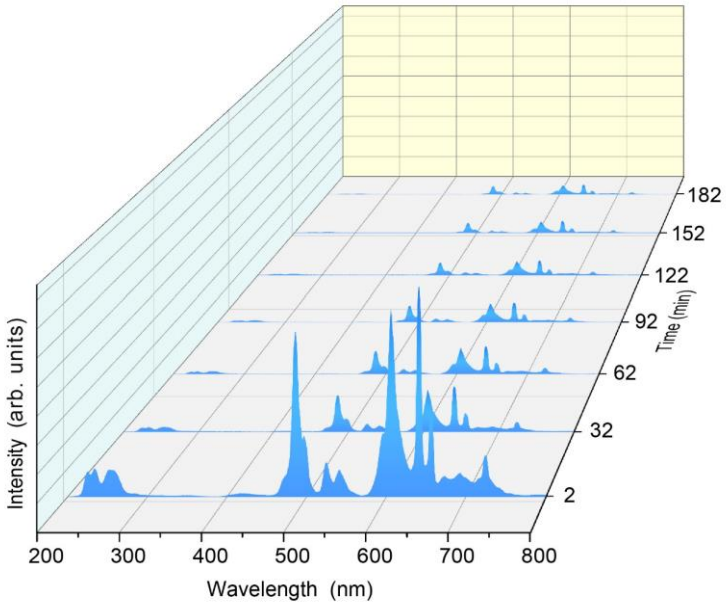

Supplementary Fig. 17. PersL spectra of SrF_2:0.5%Pr^{3+} following 5 min of X-ray irradiation.

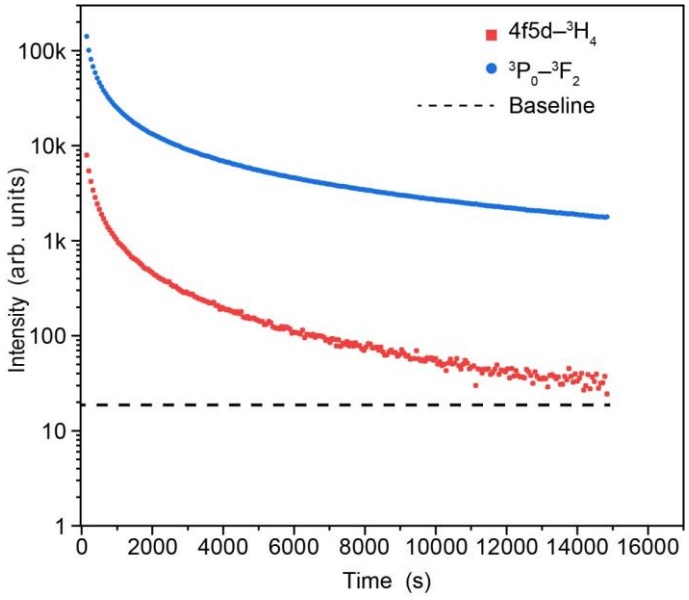

Supplementary Fig. 16. PersL decay curves of SrF_2:0.5%Pr^{3+} by monitoring the 4d5d→$^3H_4$ and $^3P_0$→$^3F_2$ transitions, following 5 min of X-ray irradiation at room temperature.

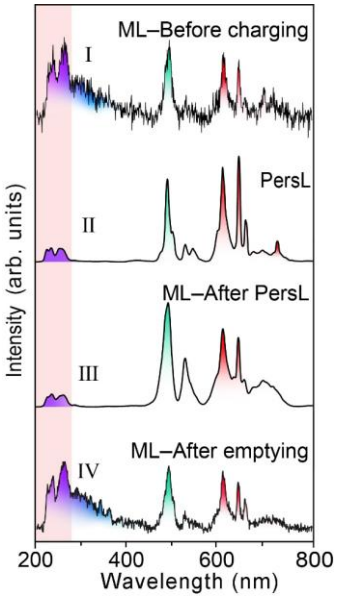

Fig. 3(b). Comparison of spectra of SrF_2:0.5%Pr^{3+} under different conditions.

Comment 4: The authors spend a lot of efforts for the demonstration of the potential applications of ML of SrF_2:$Ln^{2+,3+}$ for information encryption and high-level anti-counterfeiting, background-free marking, and structural monitoring. The similar demonstrations for potential applications of ML materials have been well documented in many previous publications. For me, the present demonstrations do not bring any new information.

Response:

We greatly appreciate the critical comment. We agree with the reviewer that information encryption or/and anti-counterfeiting demonstrations have been documented in many previous publications, such as *Nat. Commun. 2025, 16, 2378, Nat. Commun. 2024, 15, 10890, Nat. Commun. 2024, 15, 1923, Nat. Photonics 2020, 14, 760, Nat. Commun. 2022, 13, 7589, Nat. Commun. 2024, 15, 3209, Nat. Commun. 2024, 15, 3846, Nat. Mater. 2021, 20, 1539, Nat. Commun. 2022, 13, 4890, Nat. Commun. 2021, 12, 3522, Nat. Commun. 2024, 15, 5281, Nat. Commun. 2024, 15, 3053, Nat. Commun. 2020, 11, 4802*. These studies, on one hand, indicate the extreme importance of information encryption and anti-counterfeiting applications, and on the other hand, highlight the need for diverse optical materials to enhance the security levels in various application scenarios. In Fig. 5 of the manuscript, we show that our sample can render tunable visible light for information encryption, thereby providing a valuable addition to the toolbox of smart luminescent materials. To respect your opinion, we put this figure together with the related discussions into the supplementary material. In addition, we have rearranged Fig. 6 (Fig. 5 in the revised manuscript) to better illustrate the merit of the rarely reported UVC light, including background-free marking and structural monitoring. We believe these application demonstrations will attract the readers' attention and inspire them to explore more application scenarios utilizing far-UVC ML and PersL.

In summary, we have achieved unprecedented far-UVC ML as well as the widest ML wavelength span in a single host matrix that has never been achieved previously, simultaneously providing guidelines for far-UVC ML design that are expected to empower the readers to discover more superior and even customizable materials in the future. We hope the above responses can address your concerns and provide you with a clearer understanding of our work. Thank you again for your time and valuable comments!

Reviewer #3:

In this paper, the authors developed a series of SrF_2 crystals doped with various ions, including Ce^{3+}, Pr^{3+}, Nd^{3+}, Sm^{3+}, $Eu^{2+/3+}$, Gd^{3+}, Tb^{3+}, Dy^{3+}, Ho^{3+}, Er^{3+}, Tm^{3+}, and Yb^{3+}, effectively covering nearly all lanthanides known to serve as luminescent centers. These dopants enable the reported materials to exhibit mechanoluminescence (ML) across the broad wavelength range of 200–1700 nm. As noted by the reviewer, this is, to the best of our knowledge, the widest wavelength span reported within a single ML system. Furthermore, the Pr^{3+} ions in the SrF_2 host produce ML in the 200–400 nm range, with a peak at ~222 nm, representing the shortest ML wavelength reported to date.

The development of new ML materials and the extension of the ML wavelength range are critical challenges for the ML research community. This paper makes a significant contribution to both areas. Additionally, the authors demonstrated potential applications of these materials, such as information encryption, high-level anti-counterfeiting, background-free marking, and structural monitoring. Based on these findings, the paper is recommended for publication, subject to addressing the following points:

Response:

Thank you for your high recognition of our article; this will encourage us to continue to deeply engage in research and development of novel and factional optical materials. According to your invaluable comments and suggestions, we have carefully revised our manuscript. All changes are highlighted in blue in the revised manuscript, as detailed in the following point-to-point responses.

Major Comments

Comment 1: Introduction: While the authors focus on the ML of lanthanides, previous studies have shown that some transition metal ions, such as Cr^{3+}, also exhibit ML in appropriate hosts, with emission wavelengths extending to the near-infrared region. These references should be cited and discussed for completeness.

Response:

We greatly appreciate the comments. As the reviewer mentioned, transition metal ions, primarily Cr^{3+}, also exhibit ML in appropriate hosts, and the emission wavelengths are usually in the near-infrared region. There have been many researches on ML of Cr^{3+} [*J. Lumin. 2014, 154, 511; Adv. Funct. Mater. 2021, 31, 2010685; Opt. Mater. Express 2022, 12, 3238; Adv. Funct. Mater. 2023, 33, 2209275; Adv. Funct. Mater. 2023, 33, 2214497; Matter 2023, 6, 1393; ACS Appl. Mater. Interfaces 2024, 16, 33855; Small 2024, 20, 2402352, etc.*]. All the ML wavelengths of Cr^{3+} in these reports are in the range of ≈600 to 1050 nm. According to the suggestions, we have made a table to compare the emission wavelength ranges of reported mechanoluminescent systems, including these Cr^{3+}-doped ones. Please see Supplementary Table 1 for details. This table has been added to the Supplementary Information.

Comment 2: Role of Friction: The SrF_2:0.5%Pr^{3+} sample shows weak ML before X-ray exposure. The authors attribute this to local piezoelectric properties induced by Pr^{3+}, as evidenced by piezoresponse force microscopy (PFM). However, friction effects, which are frequently reported in ML studies, might also contribute. Additional experiments are necessary to confirm the role of friction in this phenomenon.

Response:

We greatly appreciate the comments. We completely agree with the reviewer's viewpoint and have added relevant experiments. In addition to piezoelectric effect, friction effect has recently been considered as a key mechanism for a lot of systems. We conducted a comprehensive review of the literature and summarized the criteria for the mechanism of ML (Supplementary Table 4). For one thing, if only the piezoelectric effect works, the material, such as $SrMg_2(PO_4)_2$:Eu^{2+} that has piezoelectric property, is expected to show similar ML intensity in different flexible carriers although

these flexible carriers own a big difference in triboelectricity. For another, if only the triboelectrification is in operation, the ML intensity is closely associated with the flexible carriers. And in this case, the material generally did not emit ML in the form of powder under direct stimulation of grinding. In this work, the powder $SrF_2:Pr^{3+}$ emitted ML under direct grinding (Fig. 4a). Moreover, the ML intensity depended on the carriers where $SrF_2:Pr^{3+}$ particles were embedded. The compound of $SrF_2:Pr^{3+}$@polydimethylsiloxane (PDMS) presented the strongest ML as PDMS has the best negative triboelectricity than ER (epoxy resin), PU (polyurethane), and SG (silicon resin), consistent with the previously reported results. It revealed the presence of triboelectrification.

The above discussions proved the presence of piezoelectric effect and triboelectricity, which are probably responsible for the ML from $SrF_2:Pr^{3+}$. However, at the present stage, we were still unable to clearly identify the extent of each mechanism's contribution to the final ML outcome. This will be a major focus of our future research.

Supplementary Table 4. Criteria for evaluating the mechanism of ML, summarized based on the literature.

Number	Material	PDMS	SG/SR	PU	ER	Powder	PFM	ML mechanism	References
1	$Ca_6BaP_4O_{17}$:Ce	√	○	×	×	×	○	Triboelectrification	43
2	B_3O_3-SiO_2-ZnO:Tb/Tm/Eu	√	√	×	×	×	×	Triboelectrification	136
3	$Sr_3Al_2O_5Cl_2$:Dy	√	√	×	×	×	○	Triboelectrification	36
4	$Ca_9Bi(PO_4)_7$:Ce/Bi	√	√	×	×	×	○	Triboelectrification	44
5	$SrGa_{12}O_{19}$:Cr	√	√	×	×	○	○	Triboelectrification	83
6	CaF_2:Tb	√	√	×	×	○	×	Triboelectrification	22,23
7	$Sr_5(PO_4)_3Cl$:Eu	√	√	×	×	×	○	Triboelectrification	35
8	$Sr_3Al_2O_5Cl_2$:Eu/Tb/Ce	√	√	×	×	×	○	Triboelectrification	37
9	ZnB_2O_4:Mn	√	○	○	○	×	○	Triboelectrification	140
10	$CaZnGe_2O_6$:Mn	√	√	√	×	×	○	Triboelectrification	98
11	$BaMgAl_{12}O_{17}$:Eu	√	○	○	○	○	×	Triboelectrification	68
12	$Lu_3Al_5O_{12}$:Ce	√	√	√	×	×	√	Triboelectrification	60
13	$LiNbO_3$:Pr	○	○	○	√	○	○	Piezoelectricity	116
14	$Ca_2MgSi_2O_7$:Eu	×	○	○	√	○	○	Piezoelectricity	106
15	Ga_2O_3:Cr	√	○	○	○	√	√	Piezoelectricity	135
16	MgF_2:Yb	√	√	√	√	√	√	Piezoelectricity	19
17	$SrMg_2(PO_4)_2$:Eu	√	√	√	√	√	√	Piezoelectricity	141
18	This work	√	√	√	√	√	√	Piezoelectricity and Triboelectrification	

√ Luminous × Non-luminous ○ Lacking

PDMS: Polydimethylsiloxane; SG: Silicon gel; SR: Silicon resin; PU: Polyurethane; ER: Epoxy resin; PFM: Piezoresponse force microscopy.

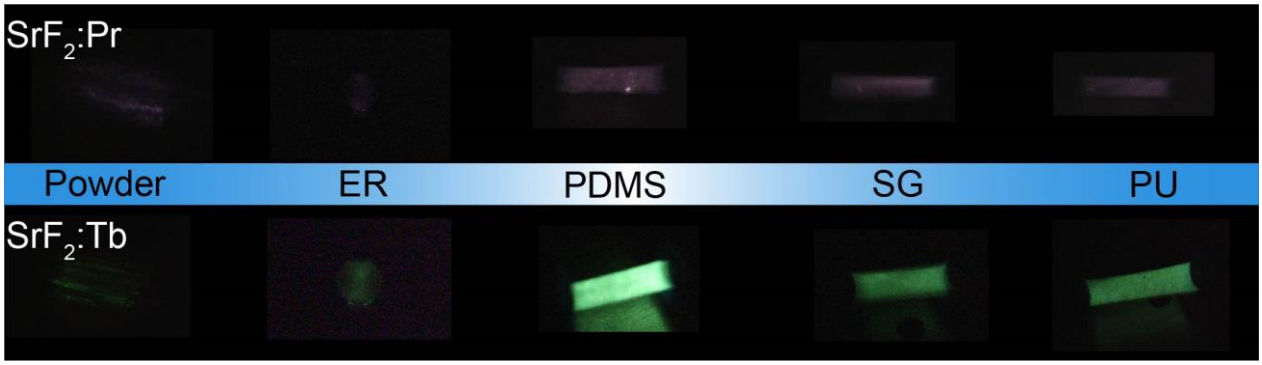

Fig. 4(a). Photographs of SrF_2:0.5%Pr^{3+} powder and SrF_2:0.5%Pr^{3+} embedded in different polymers, including ER, PDMS, SG and PU, under mechanical action.

In the 'Mechanistic investigation of multi-stimulated emission' part of 'Results' section, we have added the following sentences, 'It should be noted that, in addition to the piezoelectric effect, triboelectrification has recently been considered as another key mechanism for ML. A notable feature of triboelectrification-induced ML is that the ML intensity exhibits a strong dependence on the triboelectricity of the embedding substrates (Supplementary Table 4). Accordingly, we assessed the ML intensity of SrF_2:Pr^{3+} particles embedded in a series of polymer substrates (Fig. 4a). The results show that SrF_2:Pr^{3+}@polydimethylsiloxane (PDMS) presented the strongest ML as PDMS has the best negative triboelectricity than ER (epoxy resin), PU (polyurethane) and SG (silicon resin), consistent with the previously reported results (Supplementary Table 4). The above observations indicate that the triboelectric effect is also responsible for the ML from SrF_2:Pr^{3+}. The conclusion was further corroborated by green-emitting SrF_2:Tb^{3+} (Fig. 4a).'. Please see these changes on page 10 in the revised manuscript.

Comment 3: UV to Visible Emission Ratio: A comparison of the persistent luminescence (PersL) and ML spectra of SrF_2:0.5%Pr^{3+} reveals a change in the intensity ratio of the UV to visible bands. The authors should provide a detailed discussion of this observation, as it may yield insights into the mechanisms underlying the various emission modes.

Response:

We greatly appreciate the comments. We re-checked this figure and the original data to explain the phenomenon. The PersL spectrum in original Fig. 3b was obtained at 3 h after switching off the X-ray. The inset in the following Fig. R1 shows the enlarged UVC part, suggesting that the UVC PersL existed at this moment, but with a low signal-to-noise ratio. Supplementary Fig. 17 shows the PersL spectra of SrF_2:0.5%Pr^{3+} at different decay times. As the UVC PersL has a low initial intensity compared to the visible counterpart, it attenuates more quickly than visible light and decays to undetectable level first (Supplementary Fig. 16). To avoid ambiguity, we redrew this figure by putting the PersL spectrum obtained immediately after the stoppage of X-ray. As shown below in Fig. 3b, the UVC components of the PersL spectra are obvious to observe. Note that the ML spectrum in original Fig. 3b was obtained upon stimulation of external force at 25 N. In the updated Fig. 3b, it has been replaced by the spectrum collected at 5 N. Under such conditions, the UVC part has weakened a bit. This part has already been mentioned in the first edition of the manuscript. Please see them on pages 8 and 9 in the revised manuscript.

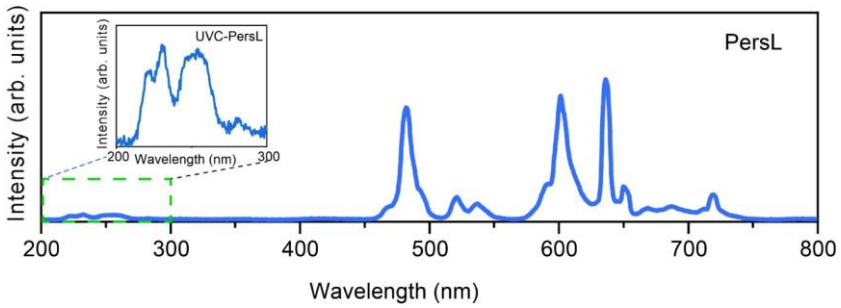

Fig. R1. PersL spectrum of SrF_2:0.5%Pr^{3+} at 3 h after switching off the X-ray.

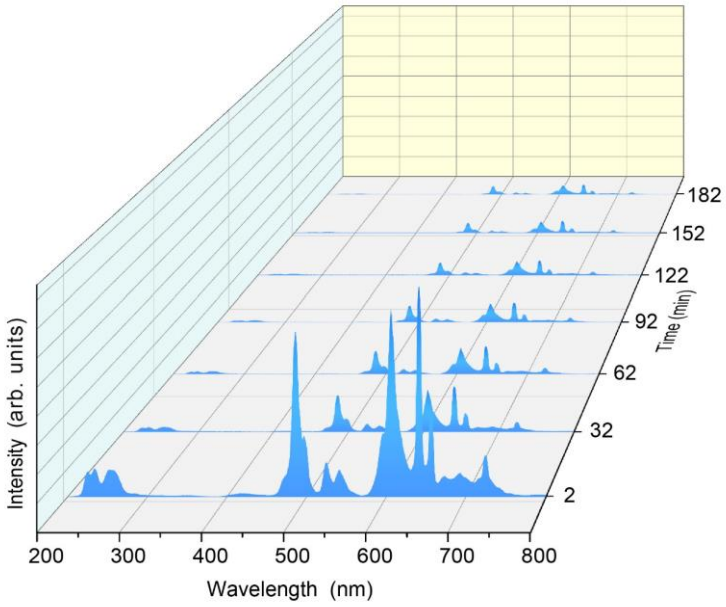

Supplementary Fig. 17. PersL spectra of SrF_2:0.5%Pr^{3+} following 5 min of X-ray irradiation.

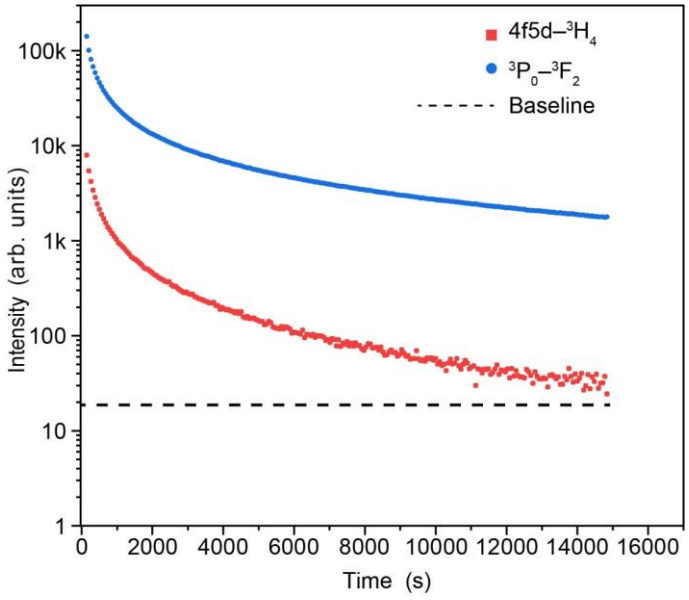

Supplementary Fig. 16. PersL decay curves of SrF_2:0.5%Pr^{3+} by monitoring the 4d5d→$^3H_4$ and $^3P_0$→$^3F_2$ transitions, following 5 min of X-ray irradiation at room temperature.

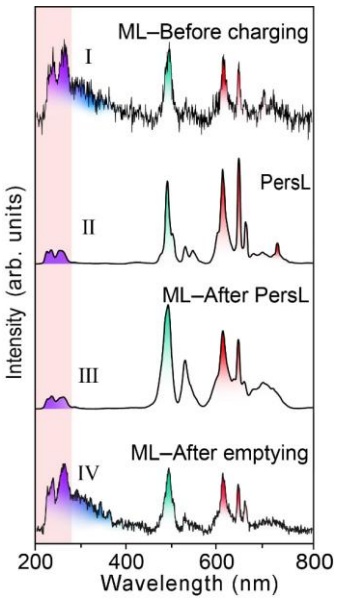

Fig. 3(b). Comparison of spectra of SrF_2:0.5%Pr^{3+} under different conditions.

Comment 4: PersL and ML Correlation: The authors state that the PersL intensity is positively correlated with the ML of SrF_2:$Ln^{2+/3+}$ (Fig. 4b). A more thorough explanation of this correlation would enhance the understanding of the relationship between these two emission phenomena.

Response:

We greatly appreciate the comments. The connection point between PersL and ML is the trapped charge carriers. As is well known, PersL is closely related to the trapped charge carriers, which can be measured by thermoluminescence (TL) technology. In this work, the trapped charge carriers would be released upon stimulation of external force, resulting in ML. Therefore, the ML is positively correlated with the TL signal and thus the PersL.

We did more experiments to verify the above discussion. As shown in Supplementary Fig. 36, the TL intensity was gradually increased by extending the X-ray pre-charging time, approaching almost saturation after 20 min of irradiation. After the release of room temperature PersL, we collected the ML spectra. As shown in Fig. 4e, the ML spectra were gradually increased by extending the X-ray pre-charging time, very similar to the case of TL curves shown in Supplementary Fig. 36. We then integrated the ML intensity and plotted it as a function of irradiation dose. The result is presented in Fig. 4f. Obviously, the ML and TL intensities had the same dependence on the irradiation dose, indicating that the trapped charge carriers contributed to the enhanced ML. As PersL is also closely related to TL (Supplementary Fig. 37), it is not difficult to understand that the stronger the PersL, the stronger the ML typically is.

In the 'Mechanistic investigation of multi-stimulated emission' part of 'Results' section, we have added the following sentences, 'To shed more light on the multi-stimulated luminescence, the trapped charge carriers were adjusted by regulating the X-ray dose. With the increase of charging time, the ML intensified gradually (Fig. 4e). The observation is as anticipated due to the increased population in trap states, as confirmed by TL measurement (Supplementary Fig. 36). After performing the integral calculation, we clearly demonstrated the positive correlation of ML and TL intensities (Fig. 4f). As PersL is also closely related to TL, it is not difficult to understand that the stronger the PersL, the stronger the ML typically is (Supplementary Figs. 37 and 38). These observations provided additional evidence that the PersL and ML originated from the same trapped charge carriers.'.

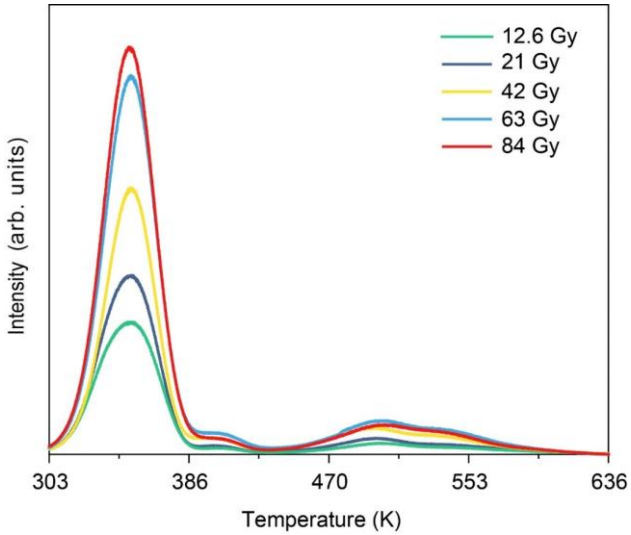

Supplementary Fig. 36. TL curves of SrF_2:0.5%Pr^{3+} after being charged by X-ray for different dose.

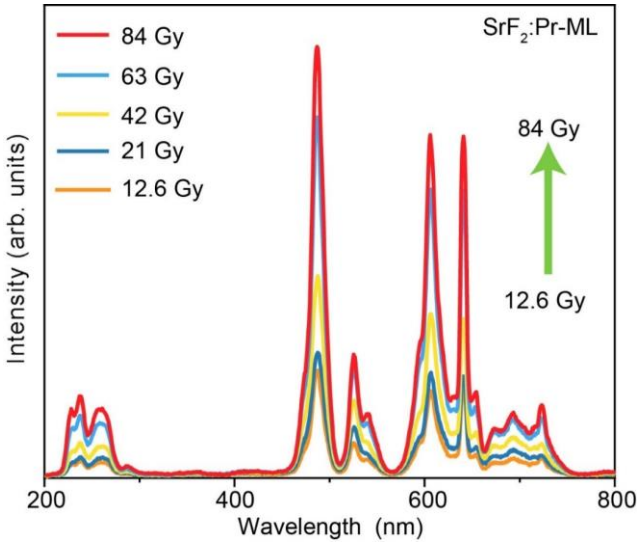

Fig. 4(e). ML spectra of SrF_2:0.5%Pr^{3+} after different X-ray exposure dose.

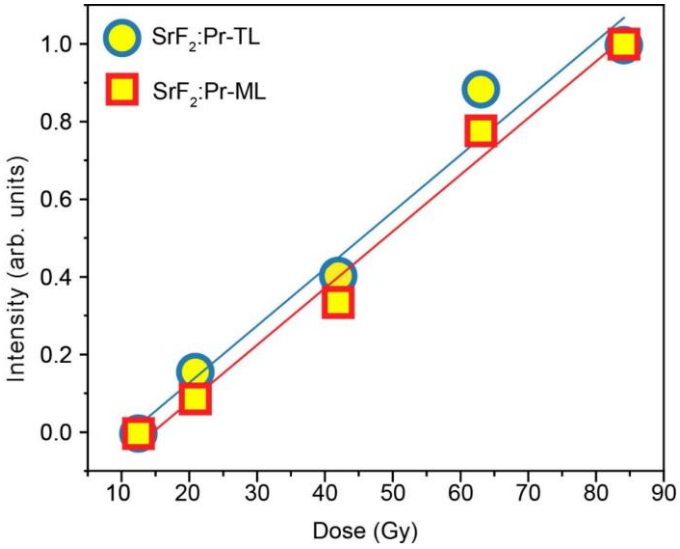

Fig. 4(f). Normalized TL and ML intensities of SrF_2:0.5%Pr^{3+} as a function of X-ray irradiation dose.

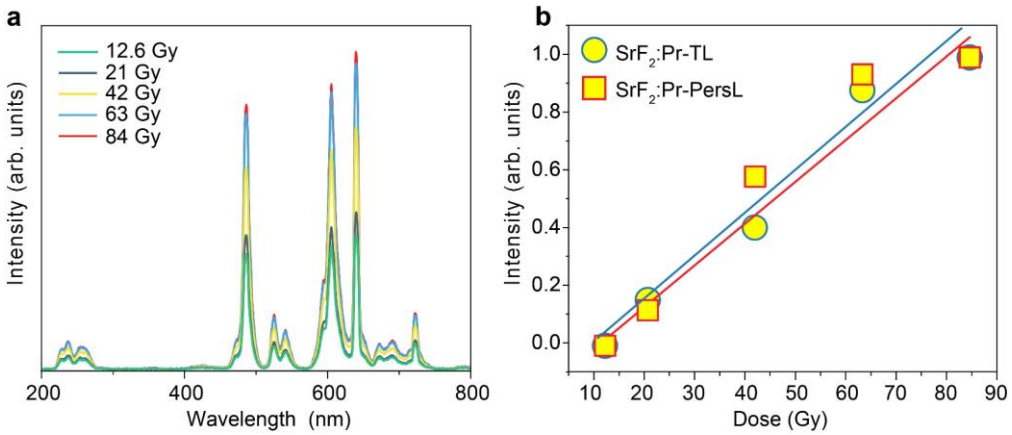

Supplementary Fig. 37. a PersL spectra of SrF_2:0.5%Pr^{3+} after being charged by X-ray of different doses, collected at 2 min after the stoppage of X-ray. **b** Comparison of normalized PersL intensity of the spectra shown in **a** and normalized TL intensity of the curves shown in Supplementary Fig. 36.

Minor Remarks

Comment 5: Figure 1: The overall tone of Figure 1 appears dim and is not visually striking. Consider enhancing the contrast or brightness to improve its appeal.

Response:

We greatly appreciate the comment. According to your suggestion, we have redrawn this figure to improve its readability, as shown below in Supplementary Fig. 1. In the revised manuscript, Supplementary Fig. 1 has been updated.

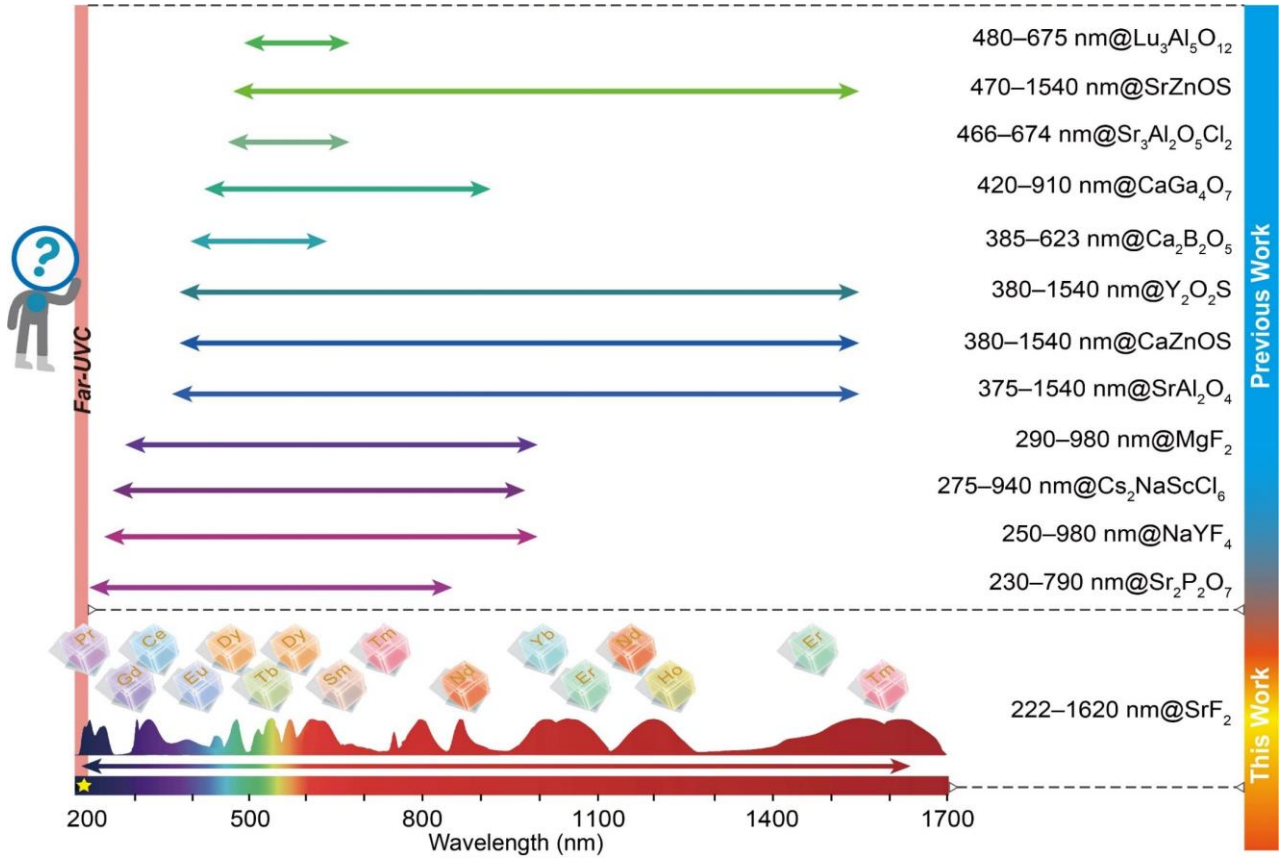

Supplementary Fig. 1. Comparison of ML spectral coverage of SrF_2 doped with lanthanides to previously reported systems.

Comment 6: Figure 3a: There should be a space between the physical quantity "h" and the number "36."

Response:

We sincerely apologize for this oversight and have separated the unit "h" and the number "36" by a space, as shown below in Fig. 3a. In the revised manuscript, Fig. 3a has been updated. To avoid similar errors, we have thoroughly checked the manuscript.

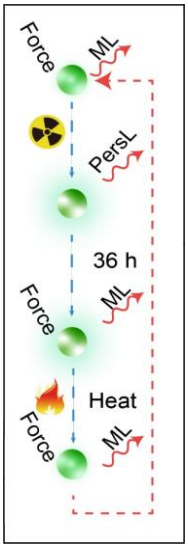

Fig. 3a. Schematic of experimental setup.

Comment 7: Figure 4e: The labels for the horizontal and vertical axes appear to be reversed. Please correct this.

Response:

We sincerely apologize for this oversight and have corrected this figure, as shown below in Supplementary Fig. 31. In the revised manuscript, Supplementary Fig. 31 (corresponding to Fig. 4e in original version) has been updated. To avoid similar errors, we have thoroughly checked the manuscript.

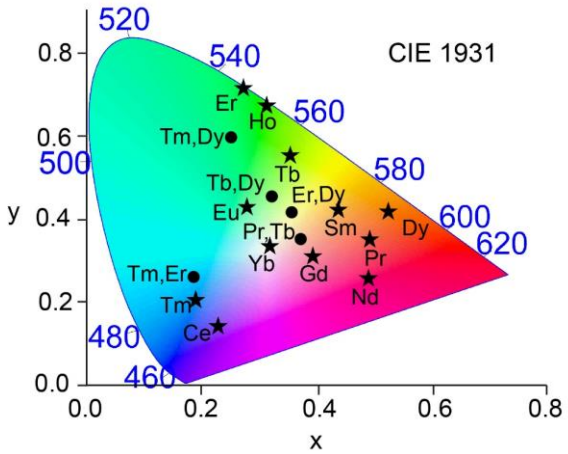

Supplementary Fig. 31. CIE chromatic coordinates of ML from SrF_2 doped with different lanthanides (doping concentration: 0.5% in molar ratio).

Point-by-point Responses (in blue) to the Reviewers' Comments (in black)

Reviewer #1:

I consider that the authors have properly addressed the comments made by referees. The paper can be accepted for publication in the present form.

Response:

Thank you once again for your support.

Reviewer #2:

The authors have addressed all my concerns and the manuscript can be accepted for publication.

Response:

Your recognition will encourage us to continue our dedicated research. Thank you!

Reviewer #3:

The authors have satisfactorily addressed all of my previous concerns, and the quality of the manuscript has been significantly improved in the revision. The broad spectral range (200–1700 nm) offers strong potential for diverse applications. I believe the manuscript is now suitable for publication in Nature Communications.

Response:

Thank you for your high recognition of our article.